HIGH-RESOLUTION MAPPING OF LITHOSPHERIC DISCONTINUITIES BETWEEN THE EASTERN CONTINENTAL MARGIN AND INTERIOR OF THE NORTH AMERICAN CONTINENT USING PKIKP AS A VIRTUAL SEISMIC SOURCE

by

MICHAEL PATRICK CUILIK

(Under the Direction of Robert B. Hawman)

ABSTRACT

Although the deployment of the US Array transportable array has enabled numerous discoveries about the crust and upper mantle, previous studies have lacked the resolution to track major discontinuities in detail. This study employs the global phase PKIKP for use in P-wave reflection analysis to improve the resolution of the Mohorovičić discontinuity and lithosphere-asthenosphere boundary (LAB) and evaluate their relationship with surface geology and physiography. The results reveal striking detail of both shallow geologic structures and the major discontinuities. We observe crustal thickening below the central and southern Appalachian Mountains and develop a new criterion for mapping the LAB based on increased reflectivity resulting from inferred drag-induced flow in the upper asthenosphere. This new criterion increases the traceability of the LAB beneath heterogeneous lithospheric settings and provides clarity on the nature of plate motion over the asthenosphere.

INDEX WORDS: Seismology, Lithosphere-Asthenosphere Boundary, Geophysics, Moho, PKIKP, P-waves, Reflection

HIGH-RESOLUTION MAPPING OF LITHOSPHERIC DISCONTINUITIES BETWEEN THE EASTERN CONTINENTAL MARGIN AND INTERIOR OF THE NORTH AMERICAN CONTINENT USING PKIKP AS A VIRTUAL SEISMIC SOURCE

by

MICHAEL PATRICK CUILIK

BS, Washington & Lee University, 2018

A Thesis Submitted to the Graduate Faculty of The University of Georgia in Partial Fulfillment of the Requirements for the Degree

MASTER OF SCIENCE

ATHENS, GEORGIA

2022

HIGH-RESOLUTION MAPPING OF LITHOSPHERIC DISCONTINUITIES BETWEEN THE EASTERN CONTINENTAL MARGIN AND INTERIOR OF THE NORTH AMERICAN CONTINENT USING PKIKP AS A VIRTUAL SEISMIC SOURCE

by

MICHAEL PATRICK CUILIK

Major Professor:	Robert Hawman
Committee:	Douglas Crowe
	Christian Klimczak

Electronic Version Approved:

Ron Walcott
Vice Provost for Graduate Education and Dean of the Graduate School
The University of Georgia
August 2022

DEDICATION

This thesis is dedicated to my family and friends for their unwavering support for my pursuit of my professional goals.

ACKNOWLEDGEMENTS

I would like to thank my advisor Dr. Hawman and my committee members Dr. Doug Crowe and Dr. Christian Klimczak for their guidance throughout my graduate program, my Washington and Lee geology professors for building the foundation for me to pursue a postgraduate degree and inspiring my love for the geosciences, my former boss Raymond J. Welder III for being a mentor and opening the door for me into the energy industry, and Chevron, the National Science Foundation (Grant #EAR-1830182), and the Joseph W. Berg Fund for funding my research.

TABLE OF CONTENTS

LIST OF TABLES

Page

LIST OF FIGURES

Page

CHAPTER 1

INTRODUCTION

Purpose of Study

Since the deployment of USArray Transportable Array (TA) across the north American continent, much progress has been made in our understanding of crustal and upper mantle structure, especially major structural features like the Mohorovičić discontinuity (Moho) and lithosphere-asthenosphere boundary (LAB) (Figure 1). However, the detailed nature of these structures and the causes of heterogeneity from the eastern continental margin to the continental interior remains enigmatic. Most work to date using the TA has involved the analysis of long wavelength features covering significant volumes of the subsurface and has primarily used S-waves (Hopper et al. 2014; Lekic et al. 2014; Long et al. 2016). To overcome some of the limitations of previous TA work, this study aims to apply the use of high frequency P-wave reflection analysis with the global phase PKIKP, a method first developed by Ruigrok and Wapenaar (2012), to attempt to capture higher resolution images of these features across the eastern US (Figure 2). The scientific significance of this analysis is to contribute answers to questions surrounding the nature of plate motion, and the extent to which surface geology is influenced by these discontinuities.

Key Geologic Features

The Moho is the name of the boundary between the crust and mantle. It is defined by the increase in velocity of propagating seismic waves from the crust to the mantle and ranges in

depth from 25–60 km in continental crust (Keller 2013; Verellen et al. 2020). Previous studies in the area have interpreted the Moho to exist at a depth range of 40–60 km, shallower beneath the coastal plain and at its deepest beneath the highest elevations of the Appalachian Mountains, suggesting a potential link between Moho depth and surface geology (Verellen et al. 2020; Long et al. 2019; Evans et al. 2019; Parker et al. 2013, 2015; Hawman et al. 2012) (Figure 3). Additionally, links have been made between Moho depth and subsurface geological features. Yang et al. found that Moho depths increased beneath the deepest parts of the Illinois Basin and follows a sharp gradient between the basin and the adjacent Ozark Dome (2017). The depth as well as the relative amplitude provide an important record of the tectonic and geologic history of the lithosphere (Yang et al. 2017; Parker et al. 2013; Lekic et al. 2011). By acquiring high resolution images of the Moho, we will be able to provide a more detailed explanation for broad scale changes in this discontinuity and the relationships it has with the tectonic history of the region.

The LAB is broadly defined as the rheological boundary between the relatively colder, stronger, lithosphere and weaker, hotter asthenosphere (Eaton et al. 2009; Fischer et al. 2010); the boundary between the two is commonly defined as the 1350° C isotherm. Previous work however indicates that this definition does not capture the complexity of this elusive discontinuity. Beneath the accreted terranes of the eastern continental margin and in the tectonically active western US, the LAB is defined by a sharp velocity gradient at a depths less than 130 km (Till et al. 2010; Rychert et al. 2005) (Figure 4). This is thought to be the result of either the presence of partial melt and volatiles at the base of the lithosphere, or alternatively a more hydrated asthenosphere in combination with downward decrease in chemical depletion or a change in seismic anisotropy (Till et al. 2010). Beneath cratonic lithosphere, the LAB has been

thought to represent a more purely thermal boundary that occurs over a depth range of 50 km or more (Eaton et al. 2009; Fischer et al. 2010; Foster et al. 2013). These gradients are the result of a relative lack of strong mantle upwelling (Fischer et al. 2010). A low velocity layer prevalent within much of the cratonic lithosphere in North America at roughly 100 km is seemingly coincident with what other studies have defined as LAB in the east and west of the North American continent, however this discontinuity cannot be the cratonic LAB as evidence from xenoliths indicate cold, dry lithospheric mantle to depths of at least 150 km (Fischer et al. 2010; Ford et al. 2010). Instead, others suggest that in these areas of thicker lithosphere that the LAB is instead made of many laminated discontinuities that only appear as a single discontinuity with long period filtering (Kind et al. 2015). Further, the theory of grain boundary sliding has been proposed as a model for generating a strong mid-lithospheric discontinuity such as the negative velocity layer at 100 km beneath the North America craton and a weaker LAB (Karato et al. 2012). The use of high frequency PKIKP reflection analysis may be able to provide clarity with respect to the above theories due to the ability to detect fine scale changes that longer period techniques cannot.

Mid-lithospheric discontinuities (MLD's) are a general term given to seismic features observed below the Moho, but above known or inferred LAB depths with a negative velocity gradient (Abt et al. 2010; Lekic and Fisher 2014; Hopper and Fischer 2015). There has been much debate around the source of MLD's, with some arguing that they are a record of relict subducting slabs (Hopper and Fischer 2015, Kind et al. 2015), while others propose a remnant lower boundary of the lithosphere below which the lithosphere continued to grow as the mantle continued to cool (Abt. et al. 2010). Selway et al. (2015) examined potential sources of MLD's using S-wave receiver functions and argue that the presence of low-velocity minerals, primarily

amphibole in mantle peridotite, is the most likely cause for widely imaged MLD's, but that most likely a combination of sources such as low velocity minerals, anisotropy, grain boundary sliding, and partial melt are at play depending on setting within the lithosphere and proximity to cratons or continental margins. By analyzing higher resolution data, we aim to bring clarity to what anomalies are MLD's and where the true LAB lies within the subsurface.

Study Area

This study focuses on a subset of eight TA lines, L through S, to provide broad spatial coverage across several major geologic features of interest. These lines cover an area of nearly 1.1 million square kilometers from Cape Cod, Massachusetts south to southern Virginia and areas west between northern Nebraska and southern Kansas (Figure 5). The study area traverses four major Precambrian provinces (Grenville, Granite-Rhyolite, Mazatal, and Yavapai), as well as significant historical tectonic features including the eastern continental rift boundary marked by the New York-Alabama Lineament and the coastal terranes to the east, and the mid-continent rift zone (Figure 6). Each line as well as the stations within each line are spaced at roughly 70 km to create uniform coverage across the continent.

The study area covers nearly two billion years of continent building history, starting from the Proterozoic Yavapai province on the western extent, moving through the Mazatzal province formed during the 1.6 Ga Mazatzal orogeny, the Granite-Rhyolite province that resulted from tectonism and volcanism from the 1.5-1.3 Ga Picuris orogeny, even further east through the Grenville province and successive breakup of Rodinia, and ending with the Appalachian orogeny and rift-to-drift conditions that led to the current passive margin setting (Yang et al. 2017) (Figure 7). This extensive tectonic history of continental collision and subsequent rifting is

associated with several key geologic features including the Appalachian and Illinois Basins and their surrounding arches, and the Mid-Continent Rift and Reelfoot Rift (Shen et al. 2013; Chen et al. 2015; Zhang et al. 2016; Yang et al. 2017; Chichester et al. 2018; DeLucia et al. 2019; Elling et al. 2020).

Previous Work Using PKIKP

Recent studies have employed the use of P-waves recorded by the SESAME array to analyze the proposed suture between Laurentia and Gondwana, and to investigate the structure of the lithosphere beneath the highest elevations of the Appalachian Mountains (Parker et al. 2013; Parker et al. 2015, 2016; MacDougall et al. 2015; Biryol et al. 2016; Hopper et al. 2016; Verellen et al. 2020). The use of PKIKP proved particularly robust, allowing for the interpretation of structures as shallow as 1 km and as deep as 225 km beneath the southern Appalachian orogen and coastal plain of Georgia (Verellen et al. 2020). Some key findings of this work were Moho depths that deepen toward the highest elevations of the Appalachian Mountains forming a crustal root that places the mountains in isostatic equilibrium, supporting the results of previous active source (Hawman et al. 2012) and passive source (Parker et al. 2013, 2016) studies, LAB depths between 120–135 km, and deeper reflections possibly due to layering associated with flow in the asthenosphere (Verellen et al. 2020) (Figure 8). The ability to capture such a variety of structures within the crust and upper mantle make the use of PKIKP ideal for detecting the structural changes over a vast study area.

CHAPTER 2

METHODOLOGY

Reflection seismology with PKIKP

Reflection seismology is a technique in which acoustic energy is introduced at the surface of the earth, and the produced wavefield is reflected at velocity discontinuities at angles dictated by Snell's law. Most commonly, this technique is used by petroleum exploration companies using a vibrating plate or air gun to detect hydrocarbons. This study aims to mimic this process using earthquake energy as a passive source. PKIKP (or PKPdf), the P-wave that travels through the inner core, bounces off the surface of the earth and propagates downward as plane waves with near vertical raypaths, ideal for imaging structure with shallow dips (Verellen et al. 2020) (Figure 9). It is important to note that when the direct PKIKP arrival reflects off the surface, the polarity switches, so discontinuities with a positive impedance contrast like the Moho appear negative, and vice versa. To have enough energy to effectively image the subsurface, all earthquakes used in this study have a minimum moment magnitude of 6.0. Also, to ensure minimal interference from other global phases, we focus on those earthquakes that occur in the range of 115–145° angular distance from the study area. Data from 16 earthquakes that occurred between 2011–2014 were downloaded from the Incorporated Research Institutions for Seismology (IRIS) SeismiQuery database (2000) to be used in conducting the analysis (Table 1).

Step 101

The first step in our processing workflow is run within the Seismic Analysis Code (SAC) program. This program carries out the following operations:

1. Reads each input trace
2. Removes its mean value
3. Removes any linear trend
4. Tapers the ends of each trace
5. Writes each modified trace to a new output file

These actions structure the data in a format that can be read and used in the SeismicUnix program.

Step 102

The second processing step has several functions. First, the SAC header is stripped from the traces, then all the headers are combined into separate header files that contain valuable information such as the latitude and longitude of each station and arc distance from each station to the earthquake epicenter. Note that not all the traces record the same number of samples. Ideally, this number is 8001 (200 s/0.025 s per sample plus 1) but some may only have 8000 or 7999 samples. To have the sample number of samples for each trace, we read only the first 7999 samples for every trace. Next, the traces are combined to form a gather with the westernmost station first and easternmost station last. Then, we pad each trace with two zeroed samples to lengthen them to 8001 samples. Once all the traces are the same length, we then resample the traces using a sampling interval of 0.020 s to replace the original interval of 0.025 s to match the interval used to record the SESAME data. This increases the total number of samples per trace

from 8001 to 10001. Next, we extract a shorter time window in preparation for future steps, either the first 100 or 110 s of each trace to match the time windows of the source wavelet of each earthquake, which is either -20 s – 80 s (100 s), -30 s –70 s (100 s), or -20 s – 90 s (110 s). Then the script performs bandpass filtering to attenuate noise. The gathers then are plotted, and the Seismic Unix headers are stripped to prepare for step 103.

Step 103

This step establishes a common time base for further processing. First, an estimate of the earthquake source wavelet is found by aligning the direct PKIKP arrivals by cross correlation and then stacking (summing) the traces, following the method of Langston and Hammer (2001). Since subsurface structure varies laterally, the stacking will cancel out reflections leaving the estimate of the energy emitted by the earthquake. In some cases, we were able to use source wavelets previously estimated for the SESAME data. The alignment of traces corrects for variations in topography at the location of each station and other environmental factors such as low velocity material near the surface (Figure 10).

Steps 104 & 105

These steps use deconvolution to equalize the effects of different earthquake source-time functions. Each seismogram is deconvolved by dividing its frequency spectrum by the spectrum of the source wavelet for the corresponding earthquake. The results are plotted with both positive and negative polarity for values of "alpha" between 1–5. The higher levels of alpha preserve more detail with less smoothing, revealing higher frequency reflections than the lower values of alpha. For step 104, the traces are plotted with uniform spacing. Then in step 105, blank traces

are inserted for unoccupied stations and the traces replotted using the correct relative station spacing between traces to accurately reflect the geometry of the subsurface. The result is a reflection profile for a given section of a TA line captured for one earthquake event (Figure 11).

Step 201

Prior to stacking, step 201 scales the output of each step 105 plot by the noise in the pre-arrival window before the direct PKIKP wave. First each trace is normalized by its largest amplitude, typically the peak of the direct arrival at zero time. Then, the traces are normalized by the root mean square (RMS) value of the noise in the noise window. This is done so that noisier traces contribute less to the stack than those with higher signal-to-noise ratios. The results are plotted with both positive and negative polarity, with the positive polarity plots showing each trace normalized by the maximum amplitude as done in step 105, while the negative polarity plot is not normalized to emphasize the effect of dividing by the RMS value (Figure 12). For noisier traces, the signal will be dampened with some especially noisy traces appearing like blank traces. Following step 201, any earthquakes that have side lobe artifacts from bandpass filtering are run through a second job to mute the signal four seconds before and after the direct PKIKP arrival to remove potential interference with any shallow signal in the 0–4 s range.

Step 202

The final step is to stack the results from the individual earthquakes in step 201 into a composite reflection profile for an entire TA line. Prior to plotting, the amplitudes are gradually increased by a factor equal to the square root of time to offset the effects of scattering, geometric

spreading, and intrinsic attenuation. This step is performed on the stacked gather rather than the individual earthquakes. Finally, the results are plotted with both positive and negative polarity with traces normalized by the maximum value. For the color plots, the latter normalization is not applied; this gives greater weight to portions of the stacked sections that are sampled by larger numbers of earthquakes.

CHAPTER 3

RESULTS

Single earthquakes

Some single events, particularly those with higher magnitudes, were able to produce clear signals for multiple discontinuities. For all profiles, two-way travel time is converted to depth using the velocity model outlined by Verellen et al. (2020). The value of average crustal velocity used for the Coastal Plain (6.1-6.2 km/s) incorporates the effect of low-velocity sediments (2 km/s); elsewhere, we use a value of 6.5 km/s. For Line S, earthquake 10 (α=3) has discernable reflections at 3 s, 6 s, 11 s, and 31-32 s (Figure 13). The reflection at 3 s (9 km) remains flat across stations 8-12 (38A-42A) and underlies the Ozark Plateau region of Missouri and is likely indicative of the base of the crystalline volcanic rocks underlying this geographic region. The reflection at 6 s (19 km) also remains flat and is within the Granite-Rhyolite province beneath southwestern Missouri, southern Illinois, and western Kentucky possibly indicating the transition from the more felsic rocks of this province to more dense mafic material below. Both the 11 s (36 km) reflection and the 31-32 s (116-120 km) reflection remain relatively flat across the length of the profile and are consistent with Moho and LAB depths respectively.

Moving northward, Line P (α=2) has two clear reflections, one at roughly 15 s (49 km) remaining flat at interpreted Moho depths and another at 28 s (100 km) consistent with a MLD (Figure 14).

Stacks: Line S

Line S is the southernmost line, and traverses Virginia, West Virginia, Kentucky, Illinois, Misouri, and Kansas (Table 2). The stacked profiles for Line S (Figures 15-17) reveal structure both shallow and deep. At 2 s (2 km), there is a reflection beneath the three easternmost stations interpreted as the base of coastal plain sediments (Figure 15). At 2 s (6 km) further west beneath eastern Kentucky and western West Virginia, there is a slightly east-dipping reflection that would be consistent with the geometry of the Appalachian Basin, a foreland basin deepest near the sediment source (Figure 15). Even further west at roughly the same depth there is a subtle reflection that separates from direct arrival sidelobes that is spatially consistent with the southern edge of the Illinois basin (Figure 15). Slightly deeper at roughly 5 s (16 km), there is a flat, horizontal reflection that is contained within the Granite-Rhyolite basement province and may represent an impedance contrast between the less dense felsic rock above and more mafic rock below (Figure 15).

Events interpreted as reflections from the Moho occur at 10 s (33 km) at the eastern edge of the line and deepen beneath the Appalachian Mountains, then shallow slightly, then deepen again to 15 s (49 km) westward before shallowing slightly to 13 s (42 km) beneath the far western edge of the profile (Figure 16). Below the Moho there is a less continuous but traceable reflection that deepens from 21 s (73 km) on the eastern margin to 28 s (100 km) toward the interior that is likely a MLD. At roughly 35 s (130 km), there is a change in the character of the profile with amplitudes becoming much more consistently bright and abundant. This character change may signify the transition from dry lithosphere to hydrous asthenosphere, and where the reflections are traceable may indicate drag induced flow (Figure 17).

Stacks: Line R

Line R passes through Virginia, West Virginia, Kentucky, Indiana, Illinois, Missouri, and Kansas (Table 3). Applying a lowcut filter prior to stacking, to suppress frequencies less than 0.25 Hz, improves resolution in the uppermost 10 s. There are two distinct shallow reflections at 1-2 s. The first is beneath Virginia and dips slightly inland (1-2 km), reflecting coastal plain sediments (Figure 18). The second is beneath the Appalachian Plateau, dips eastward (3-6 km), and is indicating the base of the Appalachian Basin (Figure 18). The Moho is better imaged if frequencies below 0.25 Hz are retained. It begins at 10 s (33 km) and dips westward to 15 s (49 km) beneath the Appalachians, then shallows, then deepens again to 16 s at the western edge of the profile (Figure 19). For deeper events, additional lowcut filtering again enhances resolution. A steadily westward dipping reflection begins at 25 s (94 km) beneath the eastern margin of the profile to 33 s (124 km) beneath Kansas (Figure 20). Below this reflection there is an increase in reflectivity, consistent with the pattern seen for line S.

Stacks: Line Q

Line Q crosses Delaware, Maryland, Virginia, West Virginia, Ohio, Indiana, Illinois, Missouri, and Kansas (Table 4). It contains many of the same features as lines R and S, and the depths of those features are within reasonable agreement from line to line. The three easternmost stations also cover the coastal plain and at 1 s (1 km) we again see a flat, horizontal reflection that does not progress westward past the fall line along the Virginia/Maryland border, suggesting this likely represents the base of coastal plain sediments (Figure 21). At 2 s (6 km) the base of the Appalachian Basin is visible again and is spatially consistent with the reflection in line S (Figure 21). Further west beneath Missouri, there is a reflection at 8 seconds (26 km) where the

base of the volcanics beneath the Ozark Plateau is expected to be (Figure 22). A reflection consistent with Moho depths in Line Q (Figure 23) deepens from 10 s (33 km) on the eastern edge to 15 s (49 km) beneath the Appalachian front and remains relatively flat westward across the remainder of the profile, except for a small depression beneath the Missouri/Illinois border (Figure 23). There is a group of reflections near interpreted LAB depths that reveals interesting evidence about the nature of the discontinuity moving from the continental margin to the interior. On the eastern edge, the top of the zone of increased reflectivity occurs at roughly 32 s (120 km; Figure 23) but moving westward along the profile a group of bright positive amplitude reflections occurs in a wedge that thickens toward the continental interior (Figure 24). Below this wedge, the apparent increased reflectivity of the asthenosphere appears and is continuous across the profile at this depth (Figure 24). This wedge of positive amplitude reflections perhaps indicates that the LAB is a more gradual, layered complex toward the center of continents where mantle upwelling is reduced and partial melt is less likely to occur.

Stacks: Line P

Line P crosses southern New Jersey, Delaware, Maryland, West Virginia, Ohio, Indiana, Illinois, Missouri, and Kansas (Table 5). Shallow crustal reflections occur at 1 s (1 km) beneath the two easternmost stations, 2 s (6 km) beneath the eastern panhandle of West Virginia, 1 s (3 km) beneath the Appalachian Plateau of West Virginia and Ohio, and 2 s (6 km) beneath the Illinois Basin (Figure 25). Moving north through the TA, the coastal plain region begins to narrow, and this can be seen in the decreasing number of stations that record this shallow structure. The small-amplitude reflection beneath the West Virginia eastern panhandle has a slight dip eastward indicating a potential thrust sheet beneath the Valley and Ridge region. The

reflection beneath the Illinois Basin extends from central Illinois to western Indiana and is consistent with the deeper part of the basin. At 6 s (19 km), there is a flat, horizontal reflection that runs from eastern Illinois to central West Virginia (Figure 25). This reflection covers the full extent of the Granite-Rhyolite province and may represent the transition from felsic to more mafic crust. A series of reflections interpreted as the Moho begins at 10 s (33 km) on the eastern edge of the profile, starts to dip beneath the Appalachian Mountains, and deepens to 17 s (55 km) beneath central Illinois (Figure 26). Below 30 s (112 km) on the eastern edge of the profile, the reflectivity becomes brighter, and moving west a wedge of positive amplitude reflections begins to appear and thickens to 41 s (143 km) on the western edge (Figure 27). This suggests the LAB is a sharper discontinuity to the east and changes in nature becoming layered to the west and is consistent with what is seen in Line Q.

Stacks: Line O

Line O runs from New Jersey through Pennsylvania, Ohio, Indiana, Illinois, Missouri, and Nebraska (Table 6). This line begins where the coastal plain is at its thinnest, and that is visible in the reflection at 1 s (1 km) beneath only the easternmost station (Figure 28). The base of sedimentary rocks within the Appalachian Basin is also present at roughly 1 s (3 km) in agreement with other lines (Figure 28). Events tentatively interpreted as Moho reflections show little continuity; they begin at roughly 11 s (35 km) but are difficult to interpret farther west (Figure 29). In the eastern part of the profile, the interpreted LAB is marked by an increase in reflectivity (Figure 29). Note that only a portion of the profile is shown because the signal west of Illinois was poor. An increase in reflectivity interpreted as LAB occurs at roughly 32 s (120 km) remaining flat across the profile.

Stacks: Line N

Line N extends from Long Island, New York through New Jersey, Pennsylvania, Ohio, Indiana, Illinois, Iowa, and Nebraska (Table 7). The results for Line N are generally poor due to an insufficient number of earthquakes with clear signal. Near the eastern end of the line, reflections between 0-2 s are consistent with thrust sheets beneath the Valley and Ridge region of Pennsylvania and basement beneath the Allegheny Plateau where the Appalachians turn to strike more east to west (Figure 31). The Moho was not clear in any of the stacked profiles. A well-defined increase in reflectivity interpreted as drag-induced flow in the asthenosphere begins at roughly 30 s (113 km) in the east and dips gradually to 38 s (143 km) to the west (Figures 30-31).

Stacks: Line M

Line M starts in Massachusetts, and continues through Connecticut, New York, Pennsylvania, Ohio, Indiana, Illinois, Iowa, and Nebraska (Table 8). Moho reflections do not show much continuity but sporadic reflections at 9 s, 10 s, and 14 s beneath Massachusetts, eastern Pennsylvania, and western Pennsylvania respectively are consistent with Moho depths in other lines. The faint nature of the signal in the eastern part of the line has to do with the small number of earthquakes (1-2) that cover this portion of the array (Table 8). The increase in reflectivity at roughly 30 s (112 km) is consistent with the pattern seen in other lines. Reprocessing to enhance higher frequencies shows a continuous positive amplitude reflection from 26 s (91 km) in the east to 37 s (139 km) in the west (Figure 33). The positive amplitude is consistent with a transition from faster lithosphere to slower asthenosphere.

Stacks: Line L

Line L is the northernmost line and extends from Cape Cod in far eastern Massachusetts into Rhode Island, Connecticut, New York, Pennsylvania, far southern Ontario, Michigan, Illinois, Iowa, and Nebraska (Table 9). Events interpreted as Moho reflections increase in time from 8 s (25 km) beneath Cape Cod to 18 s (60 km) beneath central Michigan (Figure 34). An increase in reflectivity interpreted as the top of the asthenosphere begins at roughly 33 s (124 km) (Figure 34). This is best imaged near the middle of the profile where structure is sampled by the most earthquakes.

CHAPTER 4

DISCUSSION

Moho

Given the nature of the Moho with its sharp velocity gradient, it is not surprising to see these results from PKIKP reflection are in general agreement with previous studies using other methods. Ps receiver function analysis done by Schmandt et al. (2015) revealed a thickening of the crust beneath the Appalachian Mountains at 35° latitude, slightly south of the area of focus for this study (Figure 35). We see this structure consistently across lines P though S, with the most rapid thickening occurring beneath the Appalachian Mountains and surrounding plateaus and piedmont. These results are also consistent with the results of previous active-source and passive-source experiments that show a localized root with crustal thicknesses approaching 60 km beneath the highest elevations of the southern Appalachians (Hawman et al. 2012; Parker et al. 2013, 2015, 2016; Hopper et al. 2016; Verellen et al. 2020). Our results indicate an ability to capture large scale changes in crustal thickness as well as more fine scale features, such as those noted by Yang et al. (2017). Specifically, they used a dense array of stations to capture a localized thickening of the crust (60 km) near the western edge of the Illinois Basin (Figure 36). In line Q, this depression is clearly defined and is spatially consistent with the western edge of the Illinois Basin (Figure 36). The ability to capture changes in both crustal and deeper discontinuities as well as shallow structure reveals the power of this methodology to relate deeper crustal structure to surface geology.

These results also reveal finer scale changes over larger areas. For example, Calo et al. (2016) provide a map of crustal thickness across the continental US (Figure 37). Their map indicates a smoothly dipping Moho from the east toward the interior of the continent, with no indication of varying thickness within the midcontinent. Our results tell a different story. In addition to the localized root beneath the Appalachians noted above, we see crustal thickness variations between 50-60 km west of the Appalachian Plateau (Figure 16; Figure 23). While this undulation does not appear to have any correlation to shallower structures or changes in topography, the ability to recognize this heterogeneity further lends credence to the power of this method to detect fine scale changes within the crust and upper mantle.

LAB

Our results provide significant insights regarding the nature of the lithosphere-asthenosphere boundary. Previous studies using Sp receiver function analysis have identified velocity reversals interpreted as this elusive boundary but have been unable to track it across great distances (Chen et al. 2018; Hopper et al. 2014; Eaton et al. 2009). Knowing that the nature of the LAB changes from continental margins to more cratonic lithosphere, relying on velocity changes alone to map this structure across great distances is insufficient. For example, Chen et al. (2018) used Sp receiver functions to map the same features as this study. In one profile at 38° latitude, roughly the same as line S of the TA, they interpret a long-period signal centered at a depth of 100 km to be an MLD (Figure 38). However, they did not capture another negative velocity gradient at 150 km, the depth to the LAB based on P-wave tomography. This led them to infer that the LAB within the continental interior is consistent with a more purely thermal boundary that occurs over several tens of kilometers, thus not generating a signal (Chen et al.

2018). We capture a reflection at the same depth as their interpreted MLD; the character of the plot does not change above or below this, which would be expected when transitioning from dry, rigid lithosphere to more fluid asthenosphere, and thus is unlikely to represent the LAB. Instead, we place the LAB at the boundary where reflectivity increases dipping east to west from 40-43 s or 150-160 km. This increased reflectivity occurs at a depth corresponding to the maximum negative gradient in shear-wave velocity in the tomography models (Chen et al. 2018); a similar result is seen for TA profiles T-Z farther to the south (Hanawalt et al. 2022). In line Q, we pick the LAB starting at 120 km to the east dipping to 150 km toward the interior of the continent where the discontinuity is more layered (Figure 39). Though both methods come to the same conclusion, the detail of P-wave reflectivity provides more insight to what is happening at the LAB.

Perhaps the most important result from this study is the ability to track the LAB beneath thickening lithosphere. A pitfall of receiver function analysis is the lack of clarity of the LAB beneath thick lithosphere (Abt et al. 2010; Fischer et al. 2010). This is due to the velocity gradient between lithosphere and asthenosphere occurring over much greater distances (50 km or more) beneath thick lithosphere compared to less than 15 km in places closer to continental margins (Till et al. 2010; Rychert et al. 2005). Whether this sharp velocity gradient is due to partial melt, presence of volatiles, or changes in anisotropy, these would all increase impedance contrast making the LAB more evident in receiver function profiles. Instead, the P-wave reflection results indicate a boundary that not only represents the transition from the lithosphere to the asthenosphere, but also provides information about what is occurring beneath the boundary and the dynamics of plate motion.

How the LAB is defined has been the topic of much debate and has usually focused on the makeup of the boundary itself. Whether it be a purely thermal boundary at the 1350° C isotherm, an accumulation of partial melt, change in anisotropy, or other theory, they all focus on the boundary itself for the definition. The results of this study lead us to present a new criterion for defining the LAB that allows us to trace it across varying lithospheric conditions. As previously mentioned, we placed the LAB where reflectivity increases. In some areas, we also noted that a zone of positive amplitude indicated a gradual transition from the top of the LAB to its base, typically occurring beneath areas west of the Appalachian Plateau. This increase in reflectivity is observed across most of the lines examined, including TA lines T-Z (Hanawalt et al. 2022), and is consistent with drag-induced flow within the upper asthenosphere. This occurs as the plate rides over top of the asthenosphere, dragging with it the upper portion of the more fluid mantle. As this happens, minerals begin to preferentially align, creating boundaries of anisotropy within the asthenosphere which generates the reflections (Foster et al. 2014). This anisotropy generates a relatively large impedance contrast thus amplifying the reflectivity of these boundaries compared to those within the lithosphere. This phenomenon has been recognized in other reflection studies (Verellen et al. 2020), but until now has not been observed tracking over 1,000 km across a continent as we see in our data. Placing the LAB at this boundary has a geologic significance in that it indicates where we see a change from more rigid to more fluid mantle, consistent with the definition of the LAB presented by Fischer et al. (2010).

One of the goals of this work was to evaluate the extent, if any, of the relationship of the LAB (and Moho) with surface geology. Of particular interest was Eocene-aged volcanism located west of Harrisonburg, Virginia between lines R and Q of the TA. Mazza et al. (2014)

suggested that the lack of an associated thermal anomaly may be the result of asthenospheric upwelling related to a lithospheric delamination post-rifting phase. Further, they suggest that this process may be responsible for dynamic topography and rejuvenation of the central Appalachian Mountains (Mazza et al. 2014). On both lines R and Q, we see the LAB ramping up from 130-150 km beneath the interior of the continent toward 100 km near the eastern margin of the continent (Figure 20; Figure 24). However, we do not see any evidence of lost lithosphere as is indicated in the schematic presented by Mazza et al. (2014) (Figure 40). This likely is a reflection of the lack of lateral resolution of the TA, as the zone of delamination is proposed to be a localized feature which would be covered by at most two TA stations. Therefore, our results cannot support one method of formation over another.

In addition to passive margin volcanism, intraplate seismicity also occurs toward the southern end of the study area in central and southwestern Virginia within the Central Virginia Seismic Zone and the Giles County Seismic Zone (Biryol et al. 2016) (Figure 40). The presence of these seismic zones is also thought to be related to lithospheric delamination, where thinned lithosphere becomes weaker and therefore more susceptible to failure (Biryol et al. 2016). As is the case with the Eocene volcanism, the TA does not have the resolution to capture any potential evidence of delamination. However, our method is shown to possess the ability to capture such a feature where lateral resolution is higher, suggesting that deployment of a “flexible array” with smaller station spacing could be used to test this hypothesis.

CHAPTER 5

CONCLUSIONS

The primary goals of this work were to map changes in the depth and character of the Moho and lithosphere-asthenosphere boundary, evaluate how those changes in structure relate to geology from the continental margins to the continental interior, and assess the ability of P-wave reflection analysis to image a vast range of structures and depths of the subsurface over a large study area. The most significant finding of this work was that P-wave reflectivity can capture increased reflectivity within the upper asthenosphere, allowing us to develop a new criterion for mapping the lithosphere-asthenosphere boundary. Importantly, this onset of increased reflectivity occurs at depths corresponding to the maximum negative velocity gradient determined by seismic tomography, further supporting our criterion for defining the LAB. Our preferred interpretation of this increased reflectivity is that the upper asthenosphere is coupled to the base of the lithosphere and is dragged with the plate, which preferentially aligns minerals creating layers of anisotropy that create strong impedance contrasts. This is the first study to capture this phenomenon in such detail and provides insight into how mantle flow accommodates plate motion. Additionally, we found that crustal thickness increases toward the continental interior with a localized root beneath the Appalachian Mountains. This finding is consistent with previous studies using both receiver functions and P-wave reflections. We were unable to make any connections between the LAB and surface geology, likely due to a lack of lateral resolution for relatively small-scale features in the design of the TA.

This methodology proved robust in the ability to image structures as shallow as 1-2 km beneath the Atlantic Coastal Plain to as deep as 250 km, well into the asthenosphere. There were indications that there may be a relationship between these shallow structures, such as the Illinois Basin, and Moho depths, but only found one such instance where this was exhibited. In general, the Moho west of the Appalachian Plateau appears to be an undulating discontinuity between 50-60 km, so potential links between depth and surface geology may be overstated.

Moving forward, P-wave reflection analysis can provide an opportunity to reevaluate results from previous studies that used less resolved methods such as tomography and receiver functions. Specifically, this method would be ideal for flexible array studies interested in relatively small-scale features such as determining the presence of lithospheric delamination beneath western Virginia where there is evidence of rejuvenated uplift and passive margin volcanism, or those interested in determining the relationship between crustal thickness and basin geometries.

Finally, the assessment of reflectivity in this study has been largely subjective. Work currently underway will adapt various measures of waveform coherence to more objectively determine the significance of variations in reflection character (phase and amplitude coherence) as a function of depth.

REFERENCES

Abt, D.L., Fischer, K.L., French, S.W., Ford, H.A., Yuan, H., & Romanowicz, B. (2010). North American lithosphere discontinuity structure imaged by Ps and Sp receiver functions. Journal of Geophysical Research, 115, B09301. https://doi.org/10.1029/2009JB006914

Biryol, C.B., Wagner, L.S., Fischer, K.M., & Hawman, R.B. (2016). Relationship between observed upper mantle structures and recent tectonic activity across the Southeastern United States. Journal of Geophysical Research: Solid Earth, 121, 3,393-3,414. https://doi.org/10.1002/2015JB012698

Calò, M., Bodin, T., & Romanowicz, B. (2016). Layered structure in the upper mantle across North America from joint inversion of long and short period seismic data. Earth and Planetary Science Letters, 449, 164-175. https://doi.org/10.1016/j.epsl.2016.05.054

Chen. C., Gilbert, H., Fischer, K.M., Andronicos, C.L., Pavlis, G.L., Hamburger, M.W., Marshak, S., Larson, T., & Yang, X. (2018). Shear velocity structure beneath the central United States: implications for the origin of the Illinois Basin and intraplate seismicity. Geochemistry, Geophysics, Geosystems, 17, 1,020-1,041. https://doi.org/10.1002/2015GC006206

Chichester, B., Rychert, C., Harmon, N., van der Lee, S., Frederiksen, A., & Zhang, H. (2018). Seismic Imaging of the North American Midcontinent Rift Using S-to-P Receiver Functions. Journal of Geophysical Research: Solid Earth, 123, 7,791-7,805. https://doi.org/10.1029/2018JB015771

Chong, M., Foster, D.A., Dutrow, B., & Bergeron, P. (2016). Detrital-zircon geochronology of the Sawtooth metamorphic complex, Idaho: Evidence for metamorphosed lower Paleozoic shelf strata within the Idaho batholith. Geosphere, 12(4), 1,136-1,153. https://doi.org/10.1130/GES01201.1

DeLucia, M.S., Murphy, B.S., Marshak, S., & Egbert, G.D. (2019). The Missouri High-Conductivity Belt, revealed by magnetotelluric imaging: Evidence of a trans-lithospheric shear zone beneath the Ozark Plateau, Midcontinent USA? Tectonophysics, 753, 111-123. https://doi.org/10.1016/j.tecto.2019.01.011

Eaton, D.W., Darbyshire, F., Evans, R.L., Grütter, H., Jones, A.G., & Yuan, X. (2009). The elusive lithosphere-asthenosphere boundary (LAB) beneath cratons. Lithos, 109, 1-22. https://doi.org/10.1016/j.lithos.2008.05.009

Elling, R.P., Stein, S., Stein, C.A., & Keller, G.R. (2020). Tectonic implications of the gravity signatures of the Midcontinental Rift and Grenville Front. Tectonophysics, 778, 228369. https://doi.org/10.1016/j.tecto.2020.228369

Evans, R.L., Benoit, M.H., Long, M.D., Elsenbeck, J., Ford, H.A., Zhu, J., & Garcia, X. (2019). Thin lithosphere beneath the central Appalachian Mountains: A combined seismic and magnetotelluric study. Earth and Planetary Science Letters, 519, 308-316. https://doi.org/10.1016/j.epsl.2019.04.046

Fischer, K.M., Ford, H.A., Abt, D.L., & Rychert, C.A. (2010). The lithosphere-asthenosphere boundary. Annual Review of Earth and Planetary Science, 38, 551-575. https://doi.org/10.1146/annurev-earth-040809-152438

Ford, H.A., Fischer, K.M., Abt, D.L., Rychert, C.A., & Elkins-Tanton, L.T. (2010). The lithosphere-asthenosphere boundary and cratonic lithospheric layering beneath Australia from Sp wave imaging. Earth and Planetary Science Letters, 300, 299-310. https://doi.org/10.1016/j.epsl.2010.10.007

Foster, K., Dueker, K., Schmandt, B., & Yuan, H. (2014). A sharp cratonic lithosphere-asthenosphere boundary beneath the American Midwest and its relation to mantle flow. Earth and Planetary Science Letters, 402, 82-89. http://dx.doi.org/10.1016/j.epsl.2013.11.018

Hanawalt, L., Cuilik, M.P, and Hawman, R. (2022), Mountain roots, lithospheric layering, and mantle flow: Imaging P-wave reflectivity beneath the eastern US, Geological Society of America Abstracts with Programs, v. 54, no. 4, https://doi.org/10.1130/abs/2022NC-374486

Hawman, R. B., Khalifa, M.O, & Baker, M.S (2012). Isostatic compensation for a portion of the southern Appalachians: Evidence from a reconnaissance study using wide-angle, three-componenty seismic soundings. Geological Society of America Bulletin, 124(3-4), 291-317. https://doi.org/10.1130/B30464.1

Hopper, E., Ford, H.A., Fischer, K.M., Lekic, V., & Fouch, M.J. (2014). The lithosphere-asthenosphere boundary and the tectonic and magmatic history of the northwestern United States. Earth and Planetary Science Letters, 402, 69-81.

Hopper, E., & Fischer, K.M. (2015). The meaning of mid-lithospheric discontinuities: a case study in the northern U.S. craton. Geochemistry, Geophysics, Geosystems, 16, 4,057-4,083. https://doi.org/10.1002/2015GC006030

Hopper, E., Fischer, K.M., Rondenay, S., Hawman, R.B., & Wagner, L.S. (2016). Imaging crustal structure beneath the southern Appalachians with wavefield migration. Geophysical Research Letters, 43, 12,054-12,062. https://doi.org/10.1130/G38453.1

IRIS Data Management Center (2000). Incorporated Research Institutions for Seismology. https://www.iris.edu/SeismiQuery

Karato, S. (2012). On the origin of the asthenosphere. Earth and Planetary Science Letters, 321-322, 95-103. https://doi.org/10.1016/j.epsl.2012.01.001

Keller, G.R. (2013). The Moho of North America: Abrief review focused on recent studies. Tectonophysics, 609, 45-55. https://dx.doi.org/10.1016/j.tecto.2013.07.031

Kind, R., Yuan, X., Mechie, J., & Sodoudi, F. (2015). Structure of the upper mantle in the north-western and central United States from USArray S-receiver functions. Solid Earth, 6, 957-970. https://doi.org/10.5194/se69572015

Langston, C. A., & Hammer, J. K. (2001). The vertical component P-wave receiver function. Bulletin of the Seismological Society of America, 91(6), 1805–1819. https://doi.org/10.1785/0120000225

Lekic, V. & Fischer, K.M. (2014). Contrasting lithospheric signatures across the western United States revealed by Sp receiver functions. Earth and Planetary Science Letters, 402, 90-98. https://doi.org/10.1016/j.epsl.2013.11.026

Lekic, V., French, S.W., & Fischer, K.M. (2011). Lithospheric thinning beneath rifted regions of southern California. Science, 334, 783-787. https://doi.org/10.1126/science.1208898

Long, M.D., Benoit, M.H., Aragon, J.C., & King, S.D. (2019). Seismic imaging of mid-crustal structure beneath central and eastern North America: Possiblly the elusive Grenville deformation? Geology, 47(4), 371-374. https://doi.org/10.1130/G46007.1

Long, M. D., Jackson, K. G., & McNamara, J. F. (2016). SKS splitting beneath Transportable Array stations in eastern North America and the signature of past lithospheric deformation. Geochemistry, Geophysics, Geosystems, 17, 2–15. https://doi.org/10.1002/2015GC006088

MacDougall, J.G., Fischer, K.M., Forsyth, D.W., Hawman, R.B., & Wagner, L.S. (2015). Shallow mantle velocities beneath the southern Appalachians from Pn phases. Geophysical Research Letters, 42, 339-345. https://doi.org/10.1002/2014GL062714

Mazza, S.E., Gazel, E., Johnson, E.A., Kunk, M.J., McAleer, R., Spotila, J.A., Bizimis, M., & Coleman, D.S. (2014). Volcanoes of the passive margin: The youngest magmatic event in eastern North America. GEOLOGY, 42(6), 483–486. https://doi.org/10.1130/G35407.1

Parker, E.H., Hawman, R. B., Fischer, K.M., & Wagner, L.S. (2013). Crustal evolution across the southern Appalachians: initial results from the SESAME broadband array. Geophysical Research Letters, 40(15), 3853-3857. https://doi.org/10.1002/grl.50761

Parker, E.H., Hawman, R. B., Fischer, K.M., & Wagner, L.S. (2015). Constraining lithologic variability along the Alleghenian detachment in the southern Appalachians using passive-source seismology. Geology, 43(5), 431-434. https://doi.org/10.1130/G36517.1

Parker, E.H., Hawman, R.B., Fischer, K.M., & Wagner, L.S. (2016). Estimating crustal thickness using SsPmp in regions covered by low-velocity sediments: Imaging the Moho beneath the Southeastern Suture of the Appalachian Margin Experiment (SESAME) array, SE Atlantic Coastal Plain. Geophysical Research Letters, 43, 9627-9635. https://doi.org/10.1002/2016GL070103

Ruigrok, E., & Wapenaar, K. (2012). Global-phase seismic interferometry unveils P-wave reflectivity below the Himalayas and Tibet. Geophysical Research Letters, 39, L11303. https://doi.org/10.1029/2012GL051672

Rychert, C.A., Fischer, K.M., & Rondenay, S. (2005). A sharp lithosphere-asthenosphere boundary imaged beneath eastern North America. Nature, 436, 542-545. https://doi.org/10.1038/nature03904

Rychert, C.A. & Shearer, P.M. (2009). A global view of the lithosphere-asthenosphere boundary. Science, 324(5926), 495-498. https://doi.org/10.1126/science.1169754

Selway, K., Ford, H.A., & Kelemen, P. (2015). The seismic mid-lithospheric discontinuity. Earth and Planetary Science Letters, 414, 45-57. https://doi.org/10.1016/j.epsl.2014.12.029

Shen, W., Ritzwoller, M.H., & Schulte-Pelkum, V. (2013). Crustal and uppermost mantle structure in the central U.S. encompassing the Midcontinent Rift. Journal of Geophysical Research: Solid Earth, 118, 4,325-4,344. https://doi.org/10.1002/jgrb.50321

Till, C.B., Elkins-Tanton, L.T., & Fischer, K.M. (2010). A mechanism for low-extent melts at the lithosphere-asthenosphere boundary. Geochemistry, Geophysics, Geosystems, 11, Q10015. https://doi.org/10.1029/2010GC003234

Verellen, D. N., Alberts, E. C., Larramendi, G. A., Parker, E. H. Jr, & Hawman, R. B. (2020). P-wave reflectivity of the crust and upper mantle beneath the southern Appalachians and Atlantic coastal plain using global phases. Geophysical Research Letters, 47, e2020GL089648. https://doi.org/10.1029/2020GL089648

Yang, B.B., Gao, S.S., Liu, K.H., Elsheikh, A.A., Lemnifi, A.A., Refayee, H.A., & Yu, Y. (2014). Seismic anisotropy and mantle flow beneath the northern Great Plains of North America. Journal of Geophysical Research: Solid Earth, 119, 1971-1985. https://doi.org/10.1002/2013JB010561

Yang, X., Pavlis, G.L., Hamburger, M.W., Marshak, S., Gilbert, H., Rupp, J., Larson, T.H., Chen, C., & Carpenter, N.S. (2017). Detailed crustal thickness variations beneath the Illinois Basin area: Implications for crustal evolution of the midcontinent. Journal of

Geophysical Research: Solid Earth, 122, 6,323-6,345. https://doi.org/10.1002/2017JB014150

Zhang, H., van der Lee, S., Wolin, E., Bollmann, T.A., Revenaugh, J., Wiens, D.A., Frederiksen, A.W., Darbyshire, F.A., Aleqabi, G.I., Wysession, M.E., Stien, S., & Jurdy, D.M. (2016). Distinct crustal structure of the North American Midcontinental Rift ffrom P Wave receiver functions. Journal of Geophysical Research: Solid Earth, 121, 8,136-8,153. https://doi.org/10.1002/2016JB013244

TABLES

Table 1- Summary of source earthquake information including date, magnitude, Lat/Long, and arc distance range from stations to epicenter in degrees

Earthquake	Date	Magnitude	Latitude (°N)	Longitude (°E)	Arc Distance Range (°)-Line L	Distance (°)-Line M	Distance (°)-Line N	Distance (°)-Line O	Distance (°)-Line P	Distance (°)-Line Q	Distance (°)-Line R	Distance (°)-Line S
1	4/11/14	7.1	-6.59	155.05	114.35-126.31	116.21-126.61	116.29-124.98	116.84-124.57	116.84-124.56	116.74-124.48	117.32-124.67	117.35-123.92
2	10/15/13	7.1	9.83	124.12	119.03126.78	121.06-127.49	120.24-127.15	121.83-127.40	121.71-127.71	124.09-128.26	124.86-128.75	123.33-129.23
3	7/7/13	7.3	-3.92	153.92	113.36-121.75	113.49-123.47	113.58-122.78	113.51-123.50	114.59-123.51	114.08-123.48	114.14-123.70	114.72-123.73
4	7/7/13	6.6	-6.02	149.72	115.43-126.03	116.10-127.75	115.47-127.09	117.96-127.82	117.33-127.22	118.55-127.86	118.63-128.09	118.04-128.14
5	4/6/13	7.0	-3.51	138.48	120.85-129.30	121.02-129.56	121.68-131.65	122.49-130.42	122.56-130.10	122.75-130.24	122.92-132.24	122.95-132.34
6	10/17/12	6.0	4.18	124.56	121.78-127.22	123.56-129.44	123.80-131.42	125.22-130.94	125.43-130.40	124.47-130.43	126.21-133.18	125.17-131.07
7	8/31/12	7.6	10.81	126.83	115.04-120.32	115.41-125.46	115.76-124.46	116.66-124.00	116.95-123.50	117.38-123.55	118.16-126.25	118.54-124.22
8	8/26/12	6.6	2.19	126.84	122.09-127.90	122.41-130.26	122.71-132.38	123.59-131.76	123.82-130.59	124.19-130.44	124.94-133.94	125.28-131.59
9	4/21/12	6.7	-1.69	134.32	118.35-124.73	119.08-134.38	119.28-132.42	120.54-131.39	121.92-127.30	122.18-127.52	122.87-128.17	123.13-128.48
10	4/17/12	6.9	-5.53	147.13	112.08-119.21	112.77-130.83	112.77-127.96	112.81-126.42	115.35-121.33	115.49-121.41	116.03-122.00	116.17-122.12
11	3/21/12	6.6	-6.22	146.00	115.11-120.48	114.51-126.36	116.43-129.21	116.34-127.68	117.23-122.61	116.74-122.69	117.32-123.29	117.46-123.41
12	2/6/12	6.7	9.92	123.22	115.99-120.82	116.73-124.66	117.17-126.47	117.55-126.15	118.34-123.73	118.71-124.11	118.96-124.79	119.44-125.31
13	12/14/11	7.1	-7.53	146.81	113.65-120.84	114.33-126.78	114.31-129.65	114.34-128.07	115.02-122.91	115.05-122.97	114.93-123.56	115.77-123.65
14	12/13/11	6.1	0.05	123.06	124.15-129.55	124.89-133.81	125.25-135.78	125.57-135.30	126.35-132.39	126.66-132.72	126.83-133.40	120.68-133.86
15	7/31/11	6.6	-3.51	144.97	111.61-117.51	111.73-125.01	111.88-127.80	112.53-126.36	112.45-118.53	112.64-119.74	112.67-119.93	112.67-120.51
16	6/13/11	6.4	2.54	126.46	119.53-124.40	119.92-130.14	120.23-132.23	120.38-131.63	121.14-125.70	121.52-127.39	121.73-127.80	121.98-128.48

Table 2- Fold chart showing earthquake coverage for Line S

State	Kansas						Missouri						Illinois		Kentucky					W. VA			Virginia				
Province	GP		Central Lowland				Ozark Plateau						Interior Low Plateaus					Appalachian Plateau		V&R			Piedmont		Coastal Plain		
Line S	32A	33A	34A	35A	36A	37A	38A	39A	40A	41A	42A	43A	44A	45A	46A	47A	48A	49A	50A	51A	52A	53A	54A	55A	56A	57A	58A	59A	60A	61A
EQ1																		x	x	x	x	x	x	x	x	x	x	x	x	
EQ2													x					x	x	x	x	x	x	x	x	x	x	x	x	x
EQ3															x	x	x	x	x	x	x	x	x	x	x	x	x	x	x	x
EQ4													x		x	x	x	x	x	x	x	x	x	x	x	x	x	x	x	x
EQ5										x	x	x	x	x	x	x	x	x	x	x	x	x	x	x	x	x	x			
EQ6							x	x		x	x	x	x	x	x	x	x	x	x	x	x									
EQ7							x	x	x	x	x	x	x	x	x	x	x	x	x	x	x									
EQ8							x	x	x	x	x	x	x	x	x	x	x	x	x	x	x									
EQ9							x	x	x	x	x	x	x	x	x		x													
EQ10							x	x	x	x	x	x	x	x	x		x													
EQ11							x	x	x	x	x	x	x	x	x		x													
EQ12			x	x	x	x	x	x	x	x	x	x	x	x	x		x													
EQ13				x	x	x	x	x	x	x	x	x	x	x	x		x													
EQ14			x	x	x	x	x	x	x	x	x	x	x	x	x		x													
EQ15	x	x	x	x	x	x	x	x	x	x	x	x	x	x																
EQ16	x	x	x	x	x	x	x	x	x			x	x	x																

Table 3- Fold chart showing earthquake coverage for Line R

State	Kansas							Missouri					Illinois			Indiana		Kentucky		West Virginia				Virginia					
Province	GP		Central Lowland					Ozark Plateua					C. Lowland			Interior Low Plateaus				Appalachian Plateau				V&R		Piedmont		CP	
Line R	32A	33A	34A	35A	36A	37A	38A	39A	40A	41A	42A	43A	44A	45A	46A	47A	48A	49A	50A	51A	52A	53A	54A	55A	56A	57A	58A	58B	59A	60A	61A
EQ1																		x	x	x	x	x	x	x	x	x	x	x	x	x	x
EQ2																		x	x	x	x	x	x	x	x	x	x	x	x	x	x
EQ3														x	x	x	x	x	x	x	x	x	x	x	x	x	x	x	x	x	x
EQ4														x	x	x	x	x	x	x	x	x	x	x	x	x	x	x	x	x	x
EQ5										x	x	x	x	x	x	x	x	x	x	x	x	x	x	x				x			
EQ6										x	x	x	x	x	x	x	x	x	x	x	x							x			
EQ7							x	x	x	x	x	x	x	x	x	x	x	x	x	x	x							x			
EQ8							x	x	x	x	x	x	x	x	x	x	x	x	x	x	x							x			
EQ9							x	x	x	x	x	x	x	x	x	x	x														
EQ10							x	x	x	x	x	x	x	x	x	x	x														
EQ11							x	x	x	x	x	x	x	x	x	x	x														
EQ12			x	x	x	x	x	x	x	x	x	x	x	x	x	x	x														
EQ13			x	x	x	x	x	x	x	x	x	x	x	x	x	x	x														
EQ14			x	x	x	x	x	x	x	x	x	x	x	x	x	x	x														
EQ15	x	x	x	x	x	x	x	x	x	x	x		x																		
EQ16	x	x	x	x	x	x	x	x	x				x																		

Table 4- Fold chart showing earthquake coverage for Line Q

State	Kansas					Missouri						Illinois		Indiana			Ohio			West Virginia				VA		MD		DE
Province	GP		Central Lowland																	Appalachian Plateau				V&R		P	Coastal Plain		
Line Q	32A	33A	34A	35A	36A	37A	38A	39A	40A	41A	42A	43A	44A	45A	46A	47A	48A	49A	50A	51A	52A	53A	54A	55A	56A	57A	58A	59A	60A	61A
EQ1																	x	x	x	x	x	x	x	x	x	x	x	x	x	x
EQ2																	x	x	x	x	x	x	x	x	x	x	x	x	x	x
EQ3														x	x	x	x	x	x	x	x	x	x	x	x	x	x	x	x	x
EQ4														x	x	x	x	x	x	x	x	x	x	x	x	x	x	x	x	x
EQ5										x	x	x	x	x	x	x	x	x	x	x	x	x	x	x						
EQ6							x			x	x	x	x	x	x	x	x	x	x	x	x									
EQ7						x	x	x	x	x	x	x	x	x	x	x	x	x	x	x	x									
EQ8						x	x	x	x	x	x	x	x	x	x	x	x	x	x	x										
EQ9						x	x	x	x	x	x	x	x	x	x	x														
EQ10						x	x	x	x	x	x	x	x	x	x	x														
EQ11						x	x	x	x	x	x	x	x	x	x	x														
EQ12			x	x	x	x	x	x	x	x	x	x	x	x	x	x														
EQ13			x	x	x	x	x	x	x	x	x	x	x	x	x	x														
EQ14			x	x	x	x	x	x	x	x	x	x	x	x	x	x														
EQ15	x	x	x	x	x	x	x	x	x			x	x																	
EQ16	x	x	x	x	x	x	x	x	x			x	x																	

Table 5- Fold chart showing earthquake coverage for Line P

State	Kansas					Missouri				Illinois					Indiana		Ohio					West Virginia				MD	DE	NJ
Province	GP		Central Lowland																	Appalachian Plateau		V&R		Piedmont	CP		
Line P	32A	33A	34A	35A	36A	37A	38A	39AB	40A	41A	42A	43A	44A	45A	46A	47A	48A	49A	50A	51A	52A	53A	54A	55A	56A	57A	58A	59A	60A	61A
EQ1																	x	x	x	x	x	x	x	x	x	x	x	x	x	x
EQ2												x			x		x	x	x	x	x	x	x	x	x	x	x	x	x	x
EQ3															x	x	x	x	x	x	x	x	x	x	x	x	x	x	x	x
EQ4												x		x	x	x	x	x	x	x	x	x	x	x	x	x	x	x	x	
EQ5										x	x	x	x	x	x	x	x	x	x	x	x	x	x	x						
EQ6										x	x	x	x	x	x	x	x	x	x	x	x	x								
EQ7						x	x	x	x	x	x	x	x	x	x	x	x	x	x	x	x									
EQ8						x	x	x	x	x	x	x	x	x	x	x	x	x	x	x	x									
EQ9						x	x	x	x	x	x	x	x	x	x	x														
EQ10						x	x	x	x	x	x	x	x	x	x	x														
EQ11							x	x	x	x	x	x	x	x	x	x														
EQ12			x	x	x		x	x	x	x	x	x	x	x	x	x														
EQ13			x	x	x	x	x	x	x	x	x	x	x	x	x	x														
EQ14			x	x	x	x	x	x	x	x	x	x	x	x	x	x														
EQ15	x	x	x	x	x	x	x	x	x	x	x																			
EQ16	x	x	x	x	x	x	x	x	x	x																				

Table 6- Fold chart showing earthquake coverage for Line O

State	Nebraska					Missouri					Illinois						Indiana	Ohio				Pennsylvania							NJ
Province	GP					Central Lowland															Appalachian Plateau		V&R		Piedmont				CP
Line O	31A	32A	33A	34A	35A	36A	37A	38A	39A	40A	41A	42A	43A	44A	45A	47A	48A	49A	50A	51A	52A	53A	54A	55A	56A	57A	58A	59A	60A	61A
EQ1																	x	x	x	x	x	x	x	x	x	x	x	x	x	x
EQ2														x			x	x	x	x	x	x	x	x	x	x	x	x	x	x
EQ3														x	x	x	x	x	x	x	x	x	x	x	x	x	x	x	x	x
EQ4														x	x	x	x	x	x	x	x	x	x	x	x	x	x	x	x	x
EQ5											x	x	x	x	x	x	x	x	x	x	x	x	x	x	x					
EQ6											x	x	x	x	x	x	x	x	x	x	x				x					
EQ7							x	x	x	x	x	x	x	x	x	x	x	x	x	x	x				x					
EQ8							x	x	x	x	x	x	x	x	x	x	x	x	x	x	x				x					
EQ9					x		x	x	x	x	x	x	x	x	x	x									x					
EQ10			x	x	x		x	x	x	x	x	x	x	x	x	x									x					
EQ11							x	x	x	x	x	x	x	x	x	x									x					
EQ12			x	x	x	x	x	x	x	x	x	x	x	x	x	x									x					
EQ13			x	x	x	x	x	x	x	x	x	x	x	x	x	x									x					
EQ14			x	x	x	x	x	x	x	x	x	x	x	x	x	x									x					
EQ15		x	x	x	x	x	x	x	x	x	x	x													x					
EQ16	x	x	x	x	x	x	x	x	x	x	x														x					

Table 7- Fold chart showing earthquake coverage for Line N

State	Nebraska			Iowa							Illinois				Indiana						Ohio						Pennsylvania						NJ	NY	
Province	GP			Central Lowland																			Appalachian Plateau		V&R							P	CP	
Line N	31A	32A	33A	34A	35A	36A	37A	38A	39A	40A	41A	42A	43A	44A	45A	46A	47A	48A	49A	50A	51A	52A	53A	54A	55A	56A	57A	58A	59A	60A	61A	62A	63A
EQ1																	x	x	x	x	x	x	x	x	x	x	x	x	x	x	x	x	
EQ2											x						x	x	x	x	x	x	x	x	x	x	x	x	x	x	x	x	x
EQ3														x	x	x	x	x	x	x	x	x	x	x	x	x	x	x	x	x			
EQ4										x	x		x	x	x	x	x	x	x	x	x	x	x	x	x	x	x	x	x	x			
EQ5										x	x		x	x	x	x	x	x	x	x	x	x	x	x	x				x				
EQ6									x	x	x	x	x	x	x	x	x	x	x	x	x			x					x				
EQ7							x	x	x	x	x	x	x	x	x	x	x	x	x	x	x								x				
EQ8						x	x	x	x	x	x	x	x	x	x	x				x				x					x				
EQ9			x	x	x	x	x	x	x	x	x	x	x	x	x	x								x					x				
EQ10			x	x	x	x	x	x	x	x	x	x	x	x	x	x								x					x				
EQ11							x	x	x	x	x	x	x	x	x	x								x					x				
EQ12			x	x	x	x	x	x	x	x	x	x	x	x	x	x								x					x				
EQ13			x	x	x	x	x	x	x	x	x	x	x	x	x	x								x					x				
EQ14			x	x	x	x	x	x	x	x	x	x	x	x	x	x								x					x				
EQ15	x	x	x	x	x	x	x	x	x															x					x				
EQ16	x	x	x	x	x	x	x	x	x	x	x													x					x				

Table 8- Fold chart showing earthquake coverage for Line M

State	Nebraska			Iowa						Illinois				Indiana			Ohio				Pennsylvania						NY	CT		MA		
Province	GP			Central Lowland																Appalachian Plateau			V&R			New England		CP				
Line M	31A	33A	34A	35A	36A	37A	38A	39A	40A	41A	42A	43A	44A	45A	46A	47A	48A	49A	50A	51A	52A	53A	54A	55A	56A	57A	58A	59A	60A	61A	62A	63A	64A	65A	66A
EQ1																x	x	x	x	x	x	x	x	x	x	x	x	x	x	x	x	x	x	
EQ2													x			x	x	x	x	x	x	x	x	x	x	x	x	x	x	x	x	x	x	x
EQ3													x	x	x	x	x	x	x	x	x	x	x	x	x		x	x		x				
EQ4										x		x	x	x	x	x	x	x	x	x	x	x	x	x	x		x	x		x				
EQ5								x	x	x	x	x	x	x	x	x	x	x	x	x	x	x	x	x										
EQ6								x	x	x	x	x	x	x	x	x	x	x	x	x			x											
EQ7					x			x	x	x	x	x	x	x	x	x	x	x	x	x			x											x
EQ8					x	x	x	x	x	x	x	x	x	x	x		x	x	x				x											
EQ9		x	x	x	x	x	x	x	x	x	x	x	x	x	x								x											x
EQ10		x	x	x	x	x	x	x	x	x	x	x	x	x	x								x											
EQ11			x	x	x	x	x	x	x	x	x	x	x		x								x											
EQ12		x	x	x	x	x	x	x	x	x	x	x	x	x	x								x											
EQ13		x	x	x	x	x	x	x	x	x	x	x	x	x	x								x											
EQ14		x	x	x	x	x	x	x	x	x	x	x	x	x	x								x											
EQ15	x	x	x	x	x	x	x	x															x											
EQ16	x	x	x	x	x	x	x																x											

Table 9- Fold chart showing earthquake coverage for Line L

State	Nebraska				Iowa							Illinois		Michigan				ON	PA	New York								CT		RI	MA	
Province	GP				Central Lowland														Appalachian Plateau								New England				CP	
Line L	31A	32A	33A	34A	35A	36A	37A	38A	39A	40A	41A	42A	43A	44A	46A	47A	48A	49A	50A	53A	54A	55A	56A	57A	58A	59A	60A	61A	61B	62A	63A	64A	65A
EQ1														x	x		x		x	x	x	x	x	x	x	x	x	x	x	x	x	
EQ2										x				x	x		x	x	x	x	x	x	x	x	x	x	x	x	x	x	x	x
EQ3														x	x	x	x	x	x	x	x	x			x							
EQ4										x		x		x	x	x	x	x	x	x	x	x			x							
EQ5									x	x	x	x	x	x	x	x	x	x	x	x	x	x										
EQ6						x			x	x	x	x	x	x	x	x	x	x														
EQ7						x			x	x	x	x	x	x		x	x	x														
EQ8						x	x	x	x	x	x	x	x	x		x	x	x														
EQ9		x	x	x	x	x	x	x	x	x	x	x	x	x																		
EQ10		x	x	x	x	x	x	x	x	x	x	x	x	x																		
EQ11					x	x	x	x	x			x	x	x																		
EQ12		x	x	x	x	x	x	x	x	x	x	x	x	x																		
EQ13		x	x	x	x	x	x	x	x	x	x	x	x	x																		
EQ14		x	x	x	x	x	x	x	x	x	x	x	x	x																		
EQ15	x	x	x	x	x	x	x	x	x	x	x																					
EQ16	x	x	x	x	x	x	x	x			x																					

FIGURES

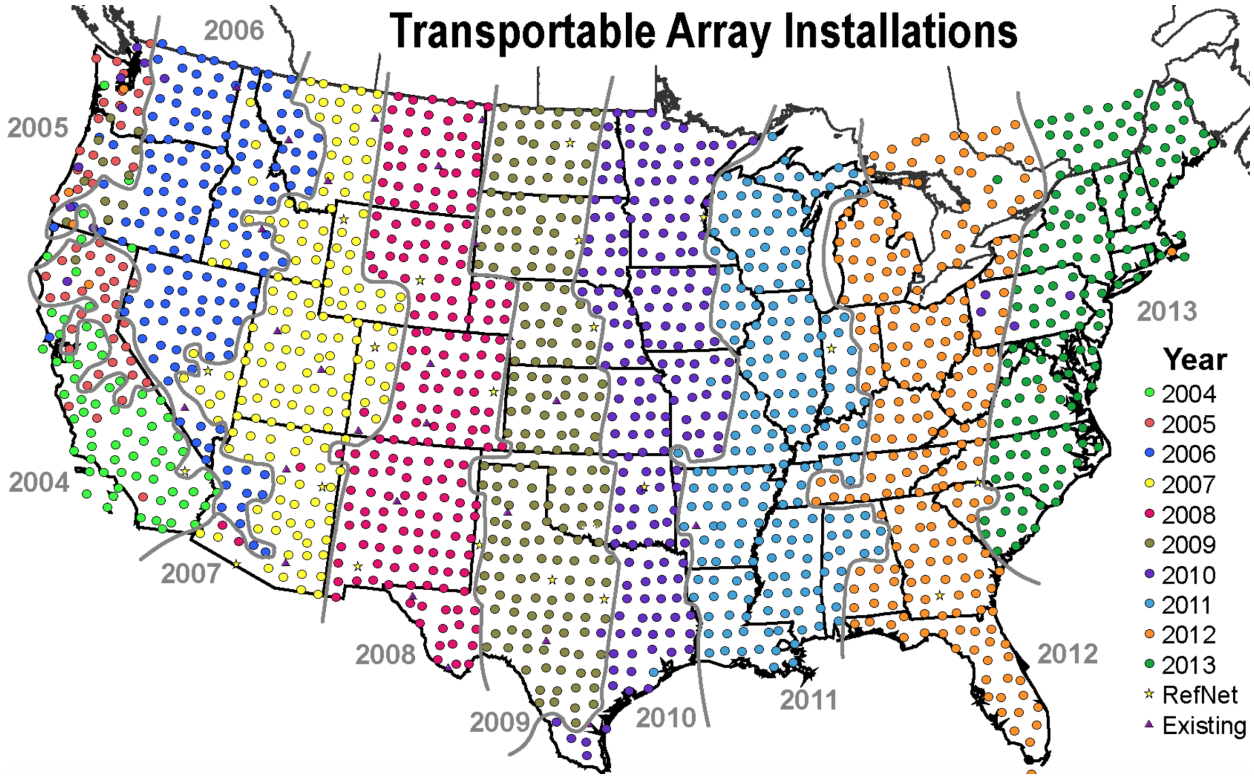

Figure 1- Map of the USArray Transportable Array (TA) with station deployment times.

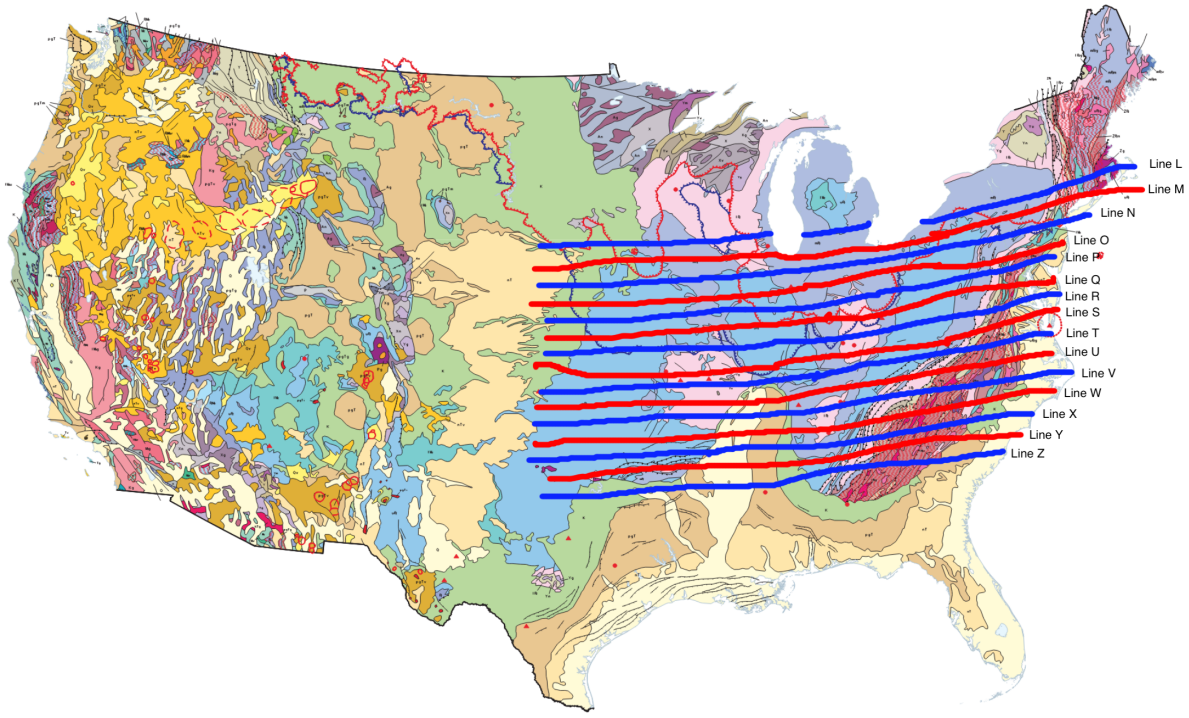

Figure 2- Map of study area from Hanawalt et al. 2022 overlain on a generalized geologic map of the continental United States.

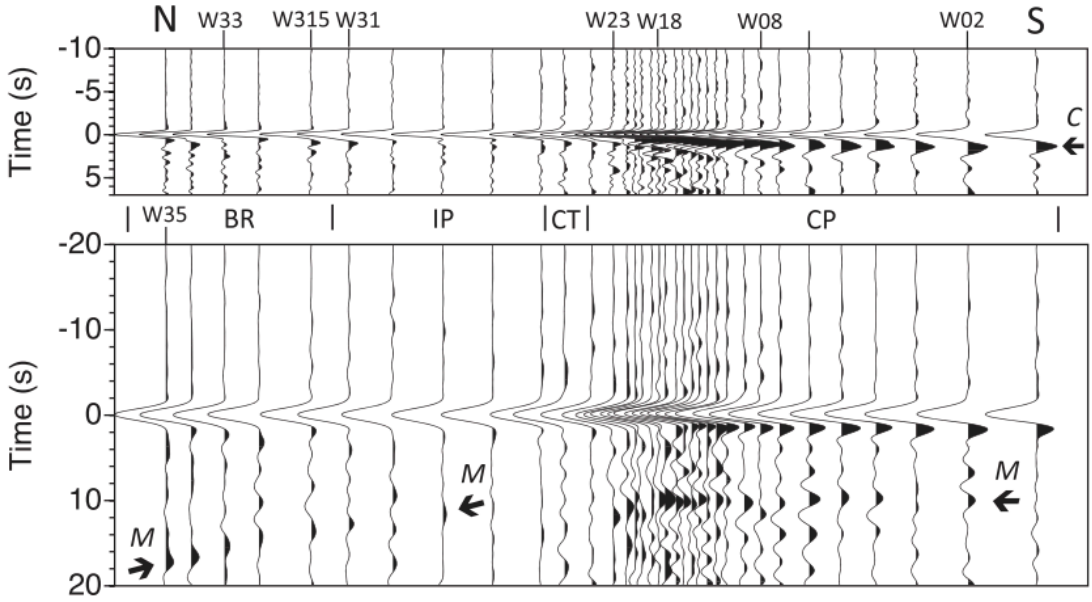

Figure 3- Stacked profile from Verellen et al. 2020. Data from the SESAME array indicate crust thickening from 10 s beneath the Coastal Plain to 17 s beneath the highest elevations of the Appalachian Mountains. C: events interpreted as primary and multiple reflections from the base of Coastal Plain sediments. M: events interpreted as reflections from the Moho

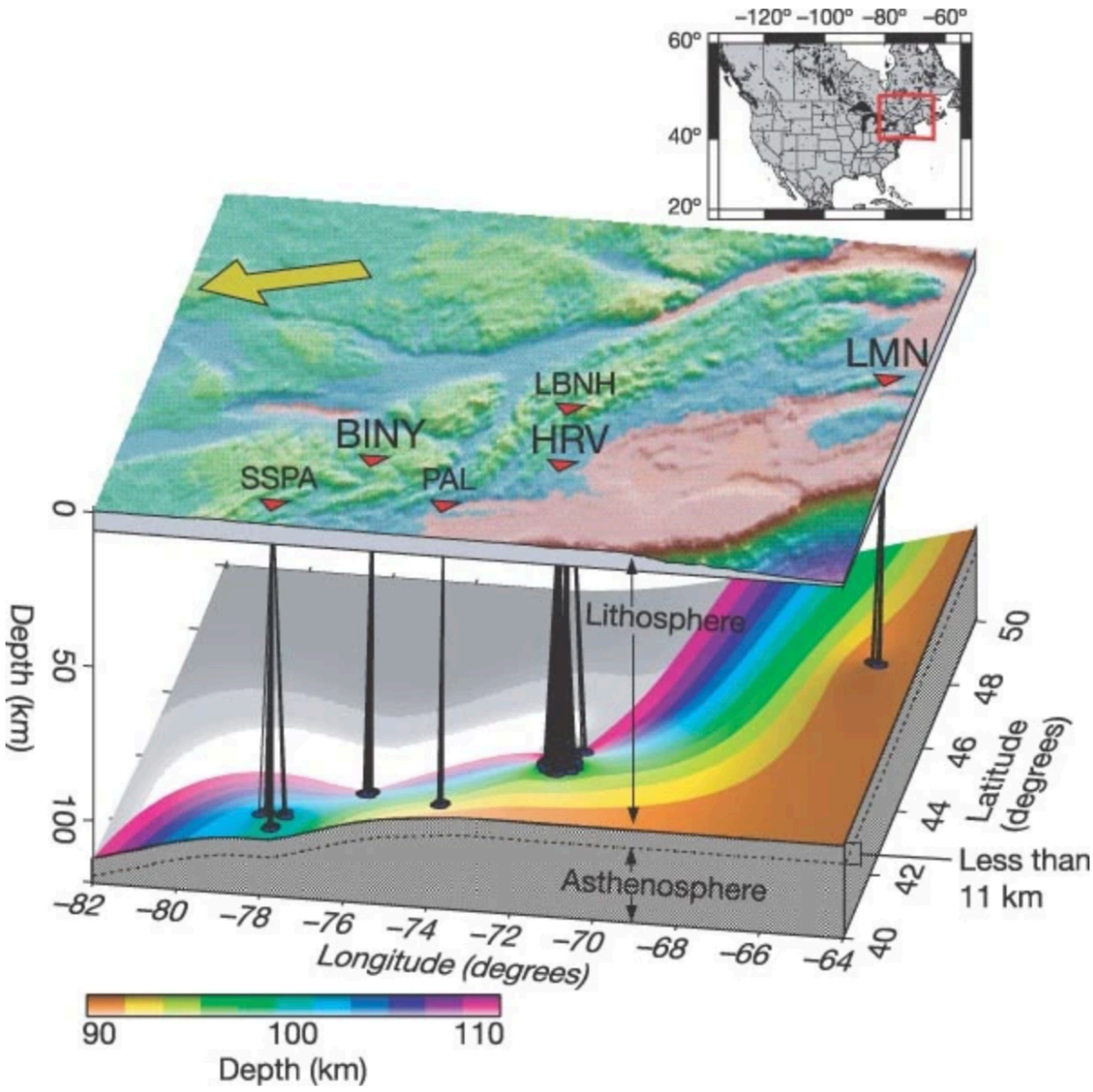

Figure 4- Three-dimensional illustration of LAB geometries from Ps waveform images near the eastern North American continental margin from Rychert et al. 2005. The figure shows a thickening of the lithosphere from 100 km to over 110 km.

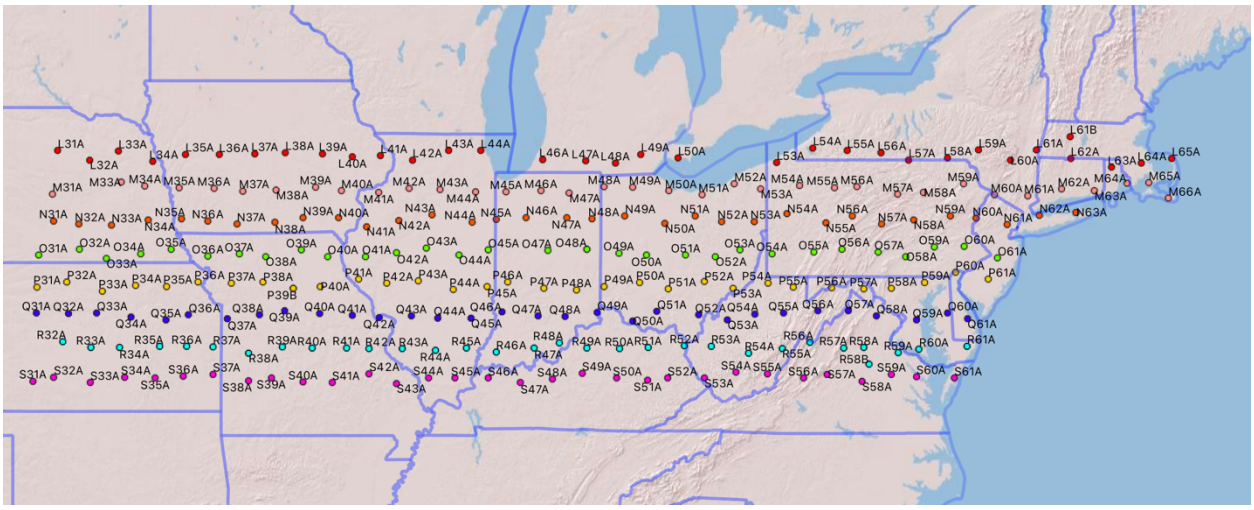

Figure 5- Map of study area

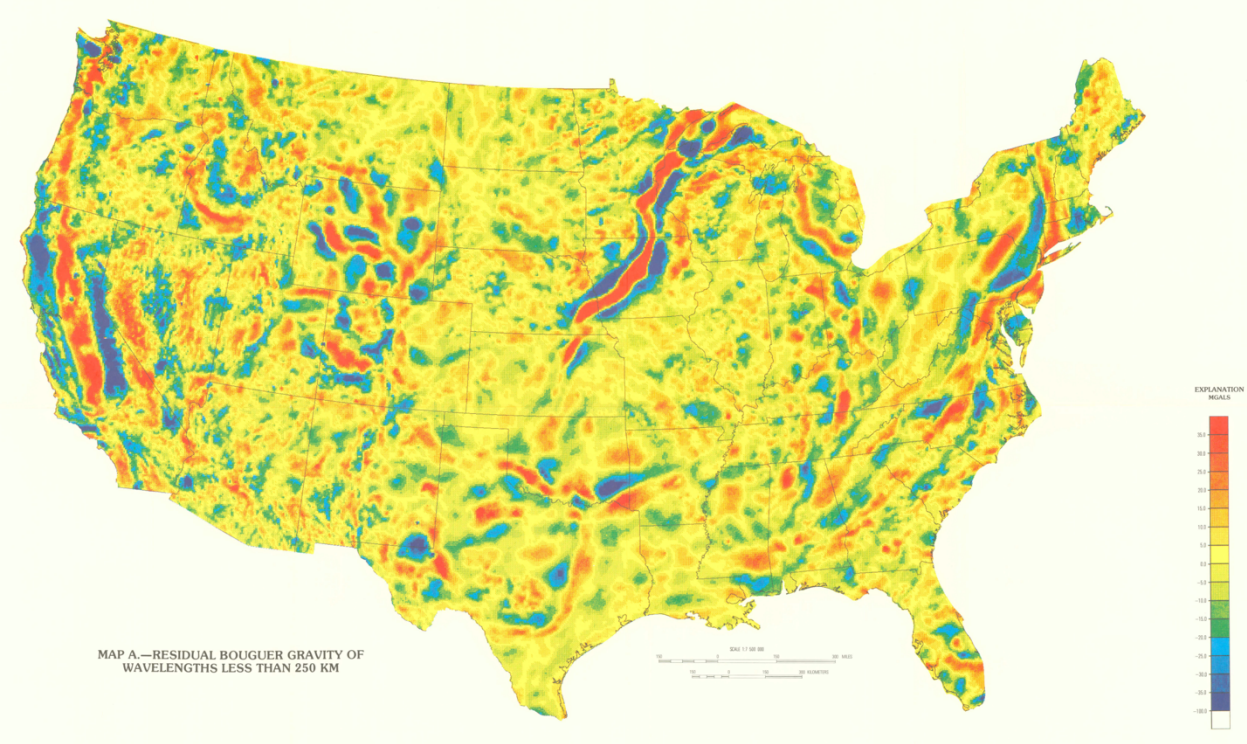

Figure 6- Bouguer gravity anomaly map (wavelength < 250 km) of the continental United States. Image provided by the USGS.

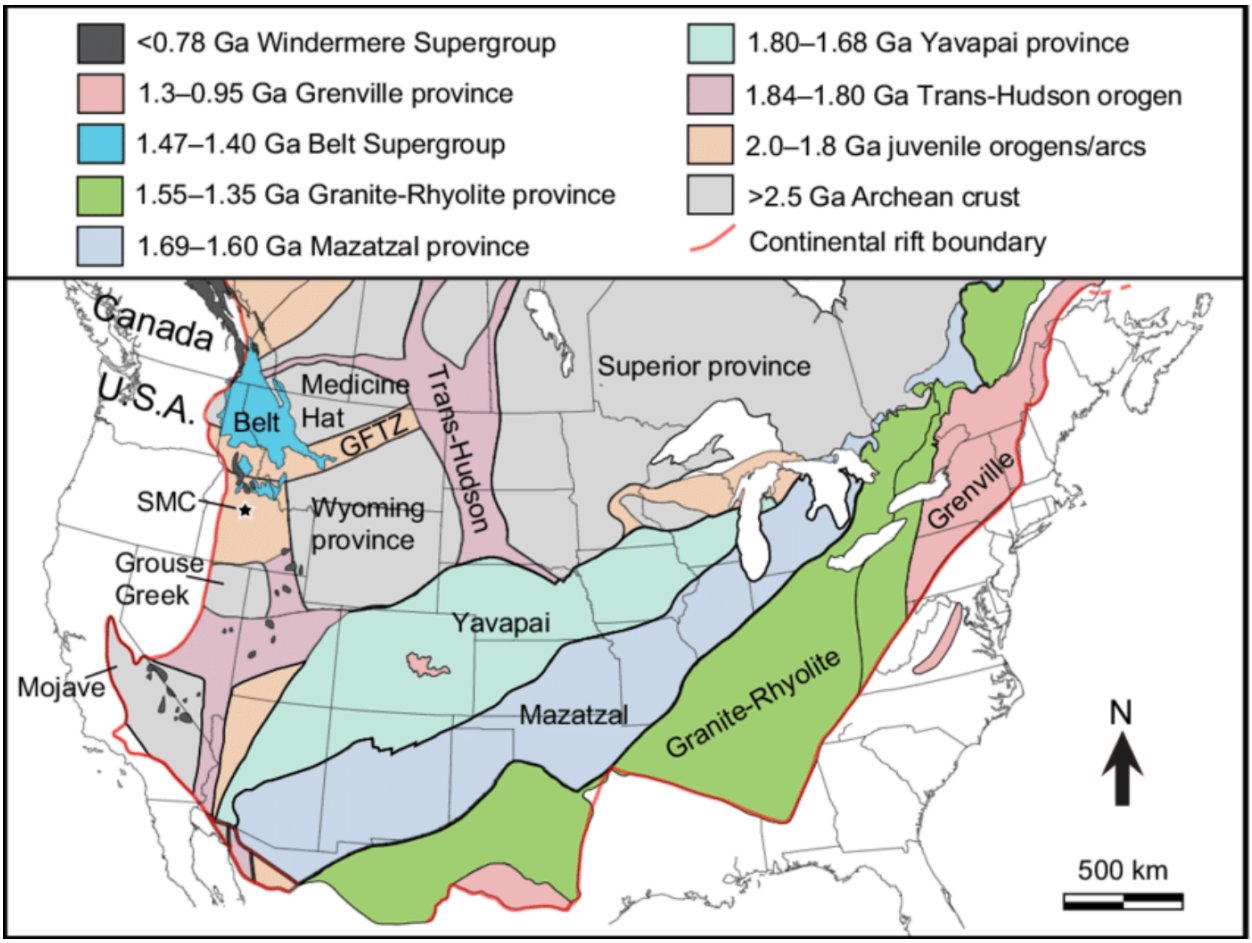

Figure 7- Map of Precambrian basement provinces of the continental United States. Image adapted from Chong et al. 2016

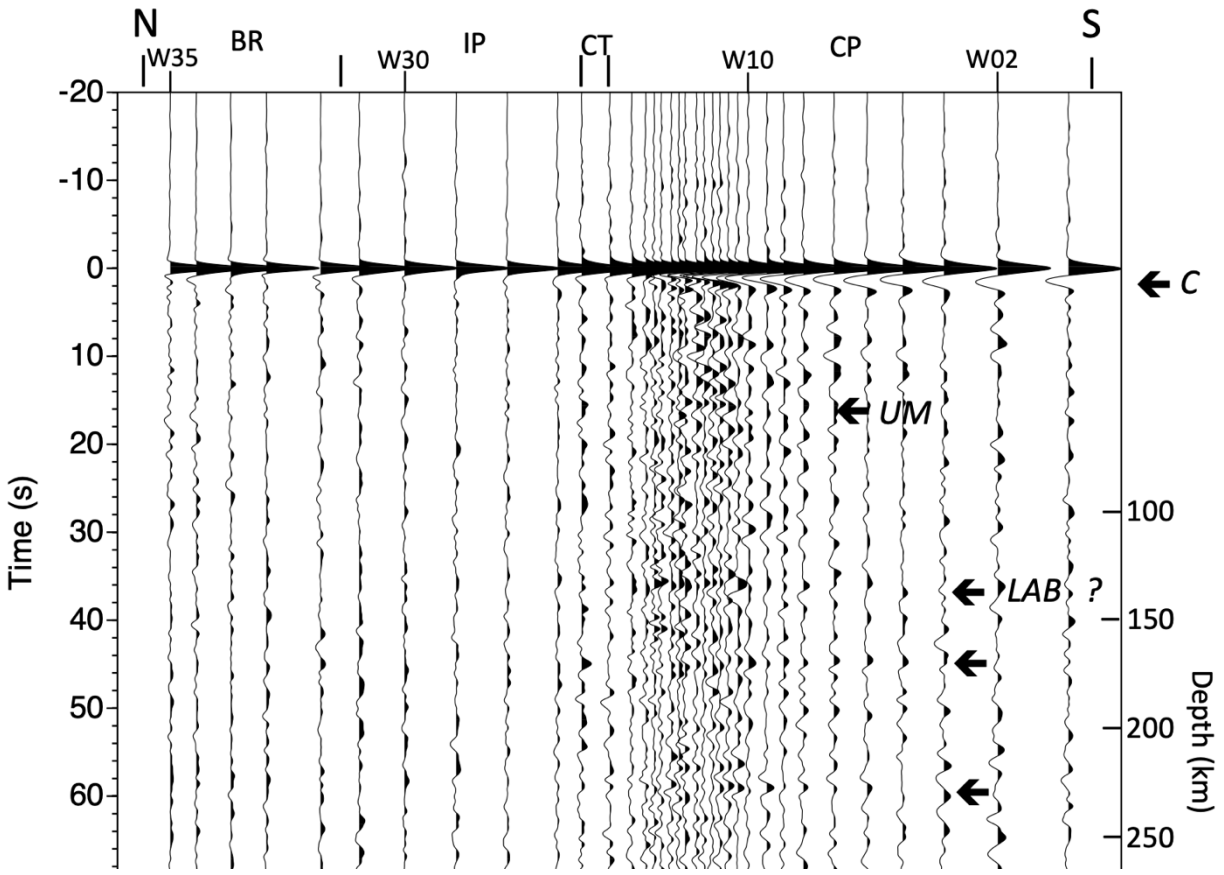

Figure 8- Stacked profile from Verellen et al. 2020. This section provides a look at the depth range at which PKIKP reflection analysis has been used to map discontinuities within the crust and mantle. C: reflections from the base of coastal plain sediments. UM: possible reflections from the subcrustal lithosphere. LAB: events interpreted as reflections from near the base of the lithosphere. Unlabeled arrows indicate events interpreted as reflections from within the asthenosphere.

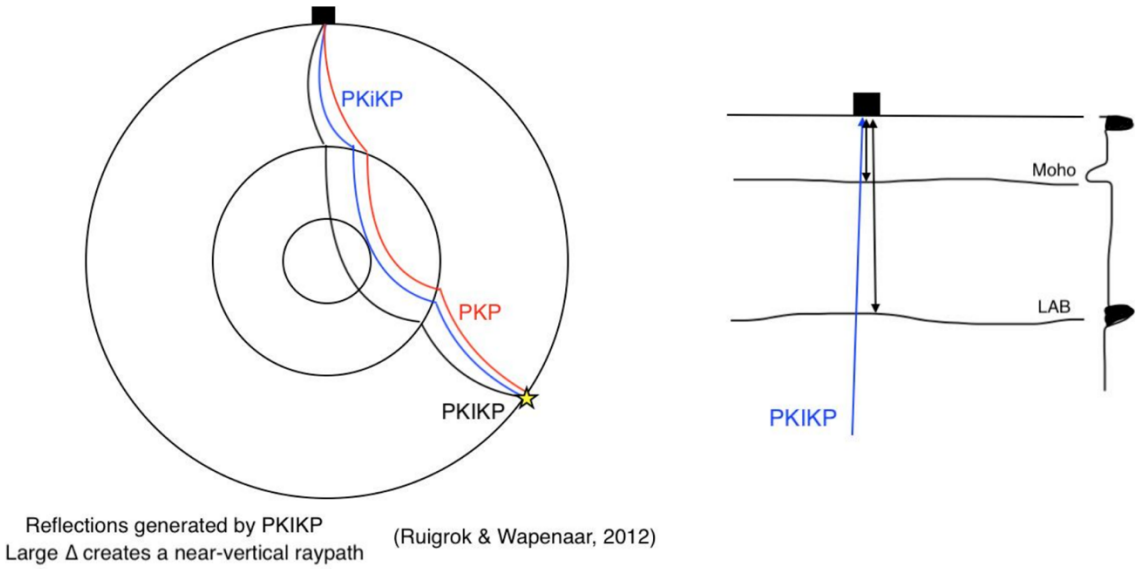

Figure 9- Diagram illustrating the raypaths of different P-wave phases through the earth. PKIKP travels through the inner core, arrives at near vertical incidence, reverses polarity and propagates back down into the subsurface where it reflects off various discontinuities

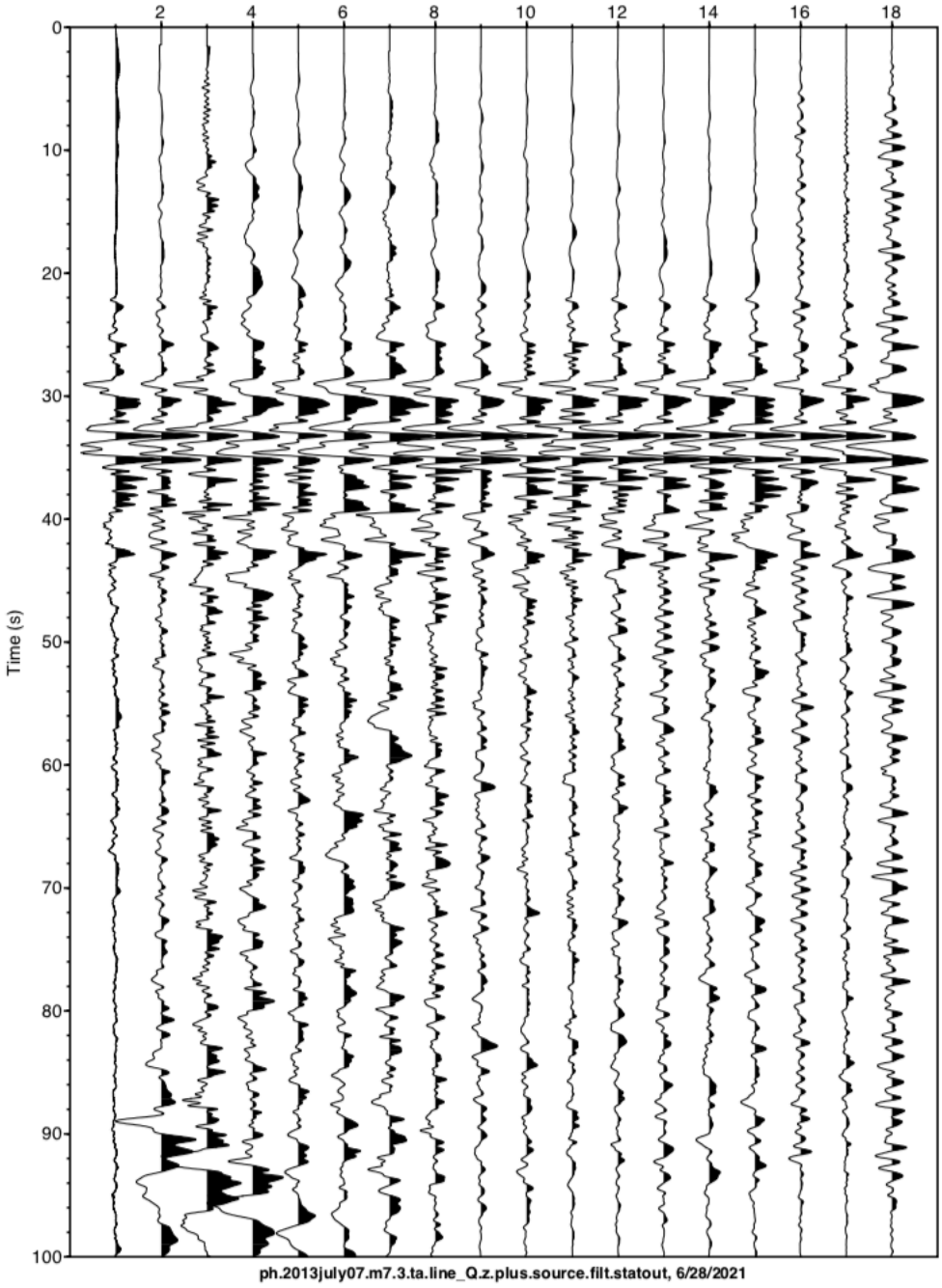

Figure 10- Plot generated by step 103 for earthquake 3 (07/07/2013 m7.3). The job aligns the PKIKP direct arrival by cross correlation, then stacks the traces together to estimate the source wavelet for the event. The source wavelet is the first trace in the gather.

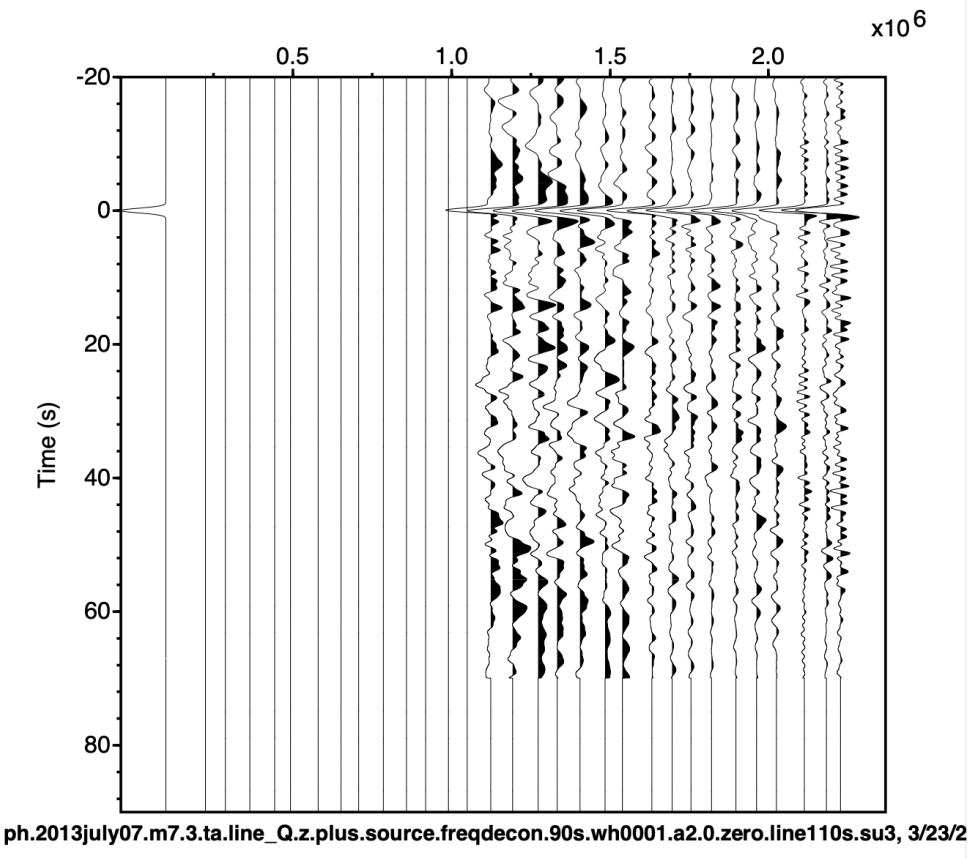

Figure 11- Example of step 105 plot for earthquake 3 (07/07/2013 m7.3). This step takes the deconvolution output from step 104 and applies the correct relative station spacing. The left-hand trace is the source wavelet deconvolved by itself.

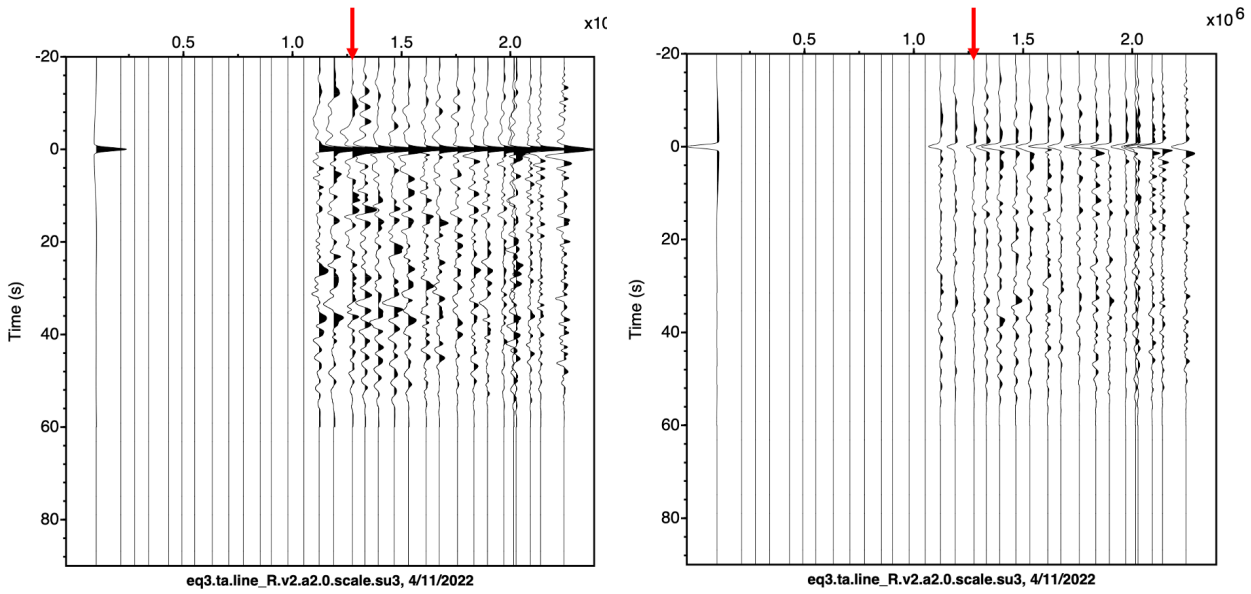

Figure 12- Side-by-side comparison of the two plots generated for each earthquake in step 201. On the left, the positive polarity plot keeps the normalized amplitudes and, on the right, the negative polarity plot that is scaled by RMS noise.

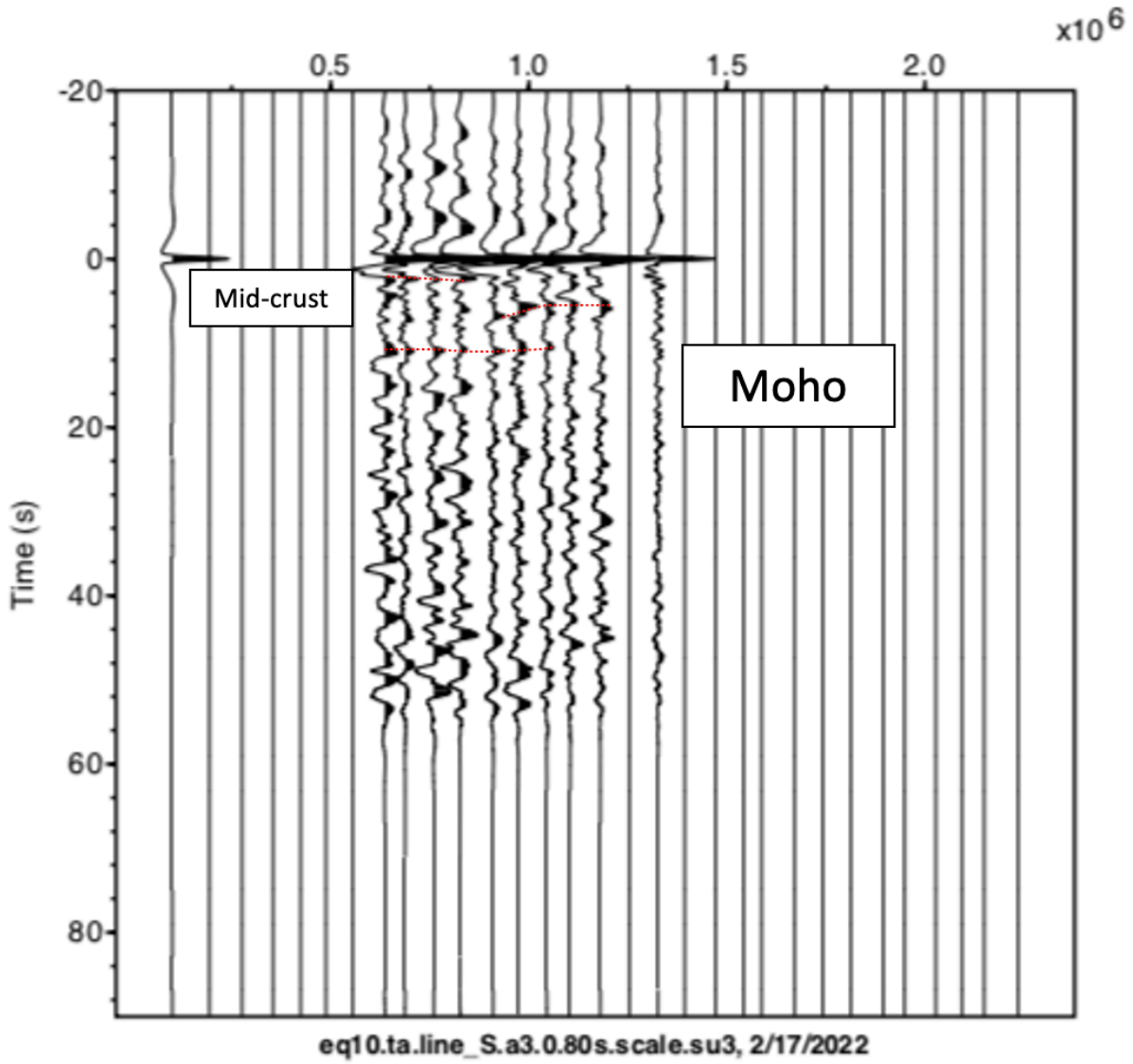

Figure 13- Results from earthquake 10 line S (04/17/2012 m6.9) α3 in positive polarity. This event generated discernable shallow signal within the crust as well as Moho at 11 seconds.

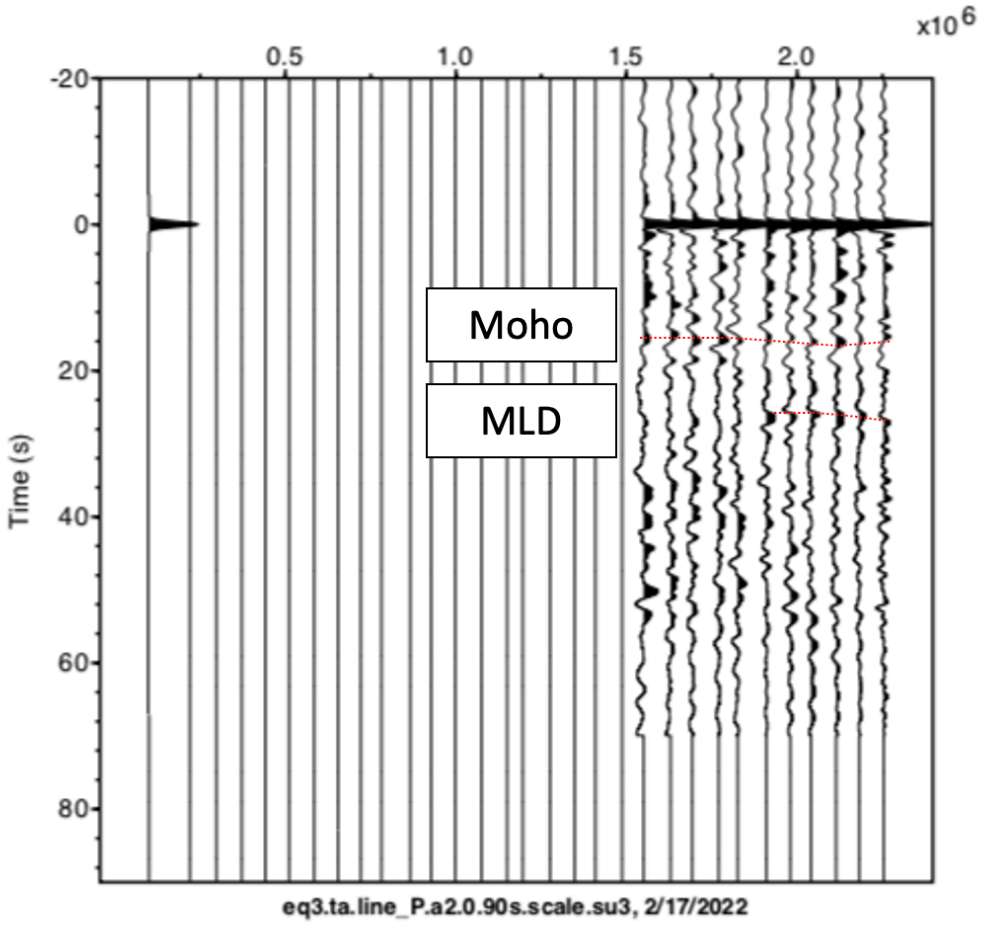

Figure 14- Results from earthquake 3 line P (07/07/2013 m7.3) α2 in positive polarity. Coherent events reflections at 15-16 seconds and 26-28 seconds are interpreted as reflections from the Moho and Mid-lithospheric discontinuity respectively.

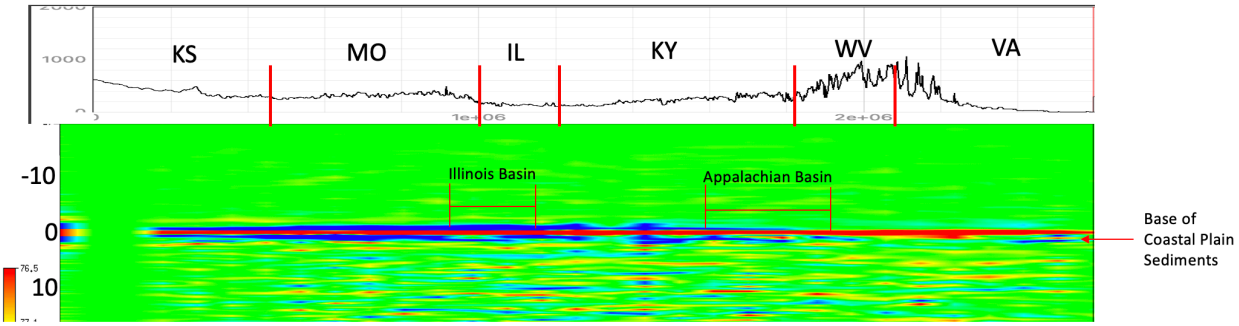

Figure 15- Stacked profile color plot for Line S α3 showing shallow structure. Marked features from east to west are the base of Paleozoic coastal plain sediments, the base of the Appalachian Basin, and the base of the Illinois Basin.

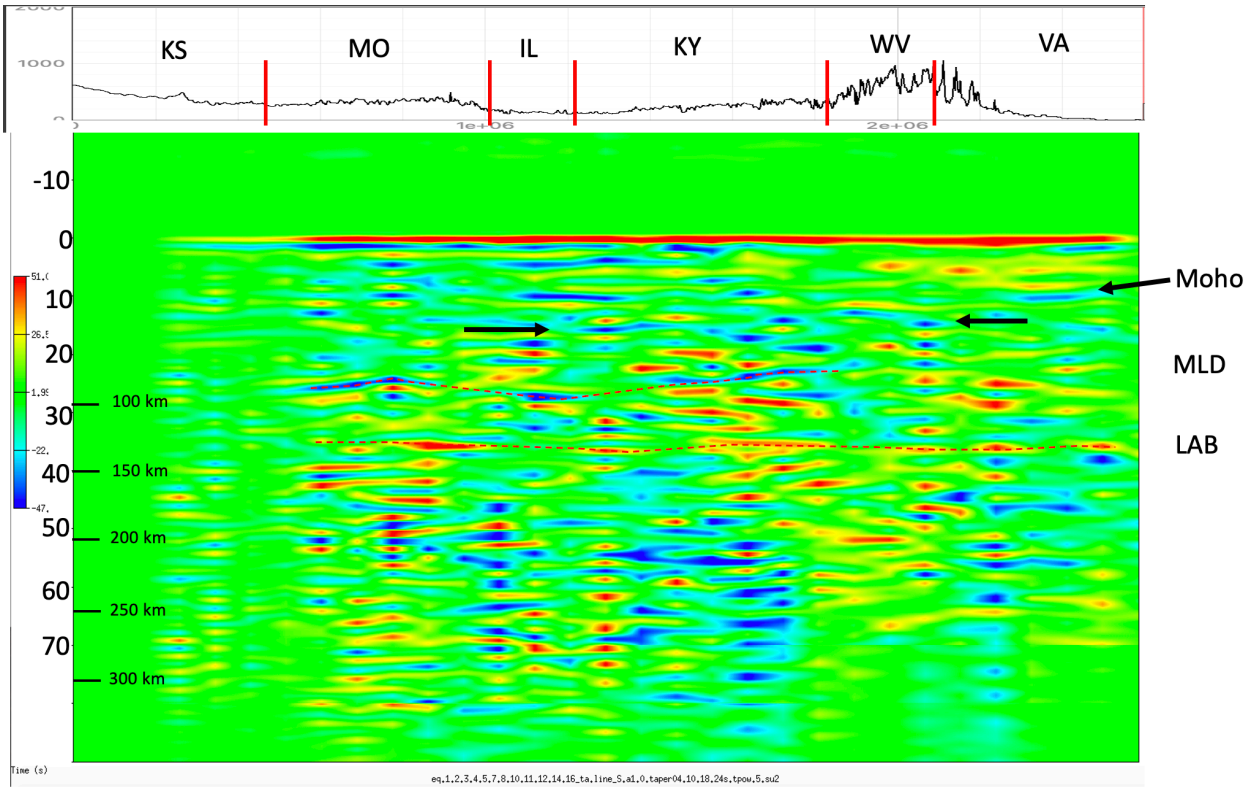

Figure 16- Stacked profile from Line S α1. Moho reflection dips from 30 km beneath the coastal plain to 55 km beneath eastern Illinois before shallowing slightly further west. Crustal thickening occurs more rapidly beneath the Appalachian Mountains. Between 85-100 km is a semi-continuous reflection that is consistent with MLD depths. The LAB is marked by the transition to increased reflectivity at roughly 130 km.

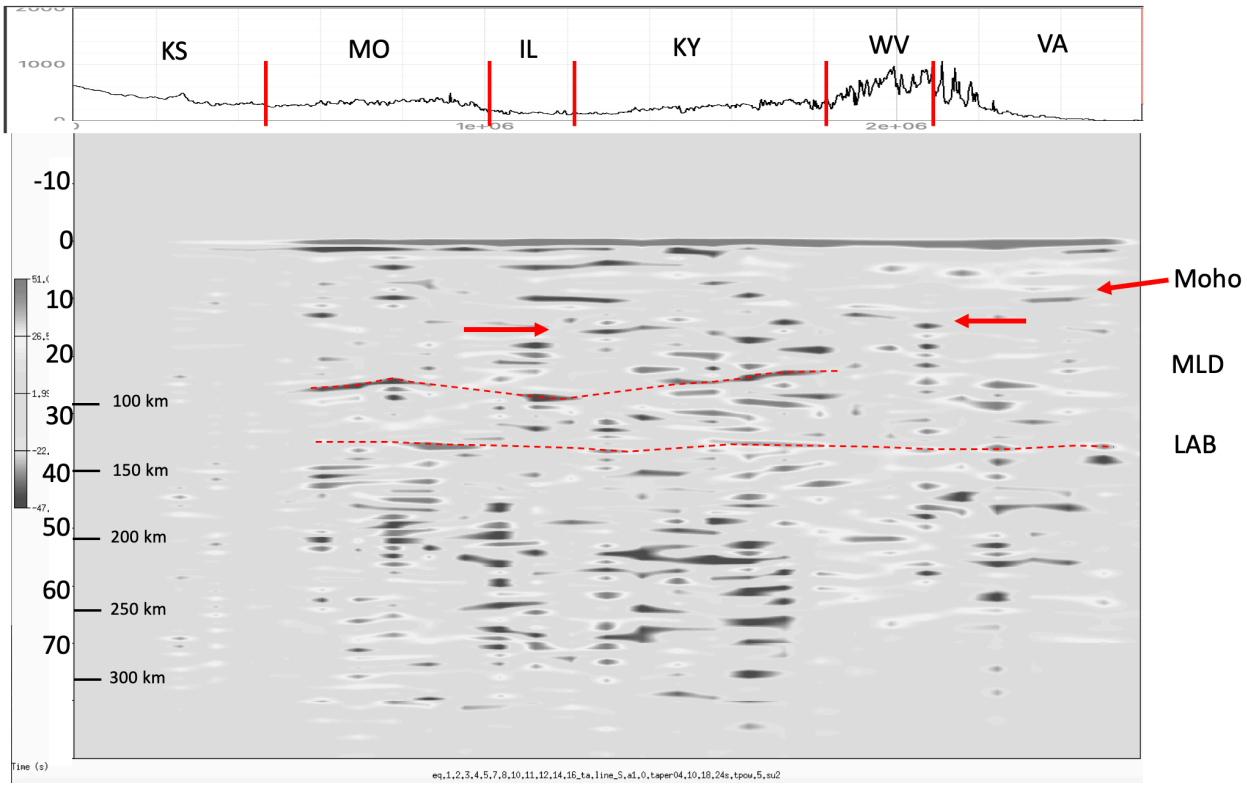

Figure 17- Black and white stacked profile of Line S α1. The black and white emphasizes the contrast between less reflective lithosphere and more reflective asthenosphere.

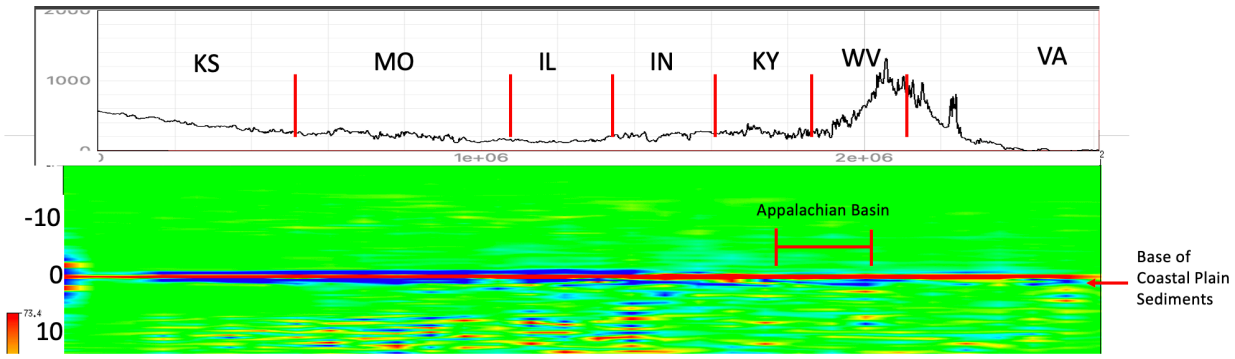

Figure 18- Stacked profile from line R α3. The two shallow structures captured in this profile are the base of Coastal Plain sediments and the Appalachian Basin.

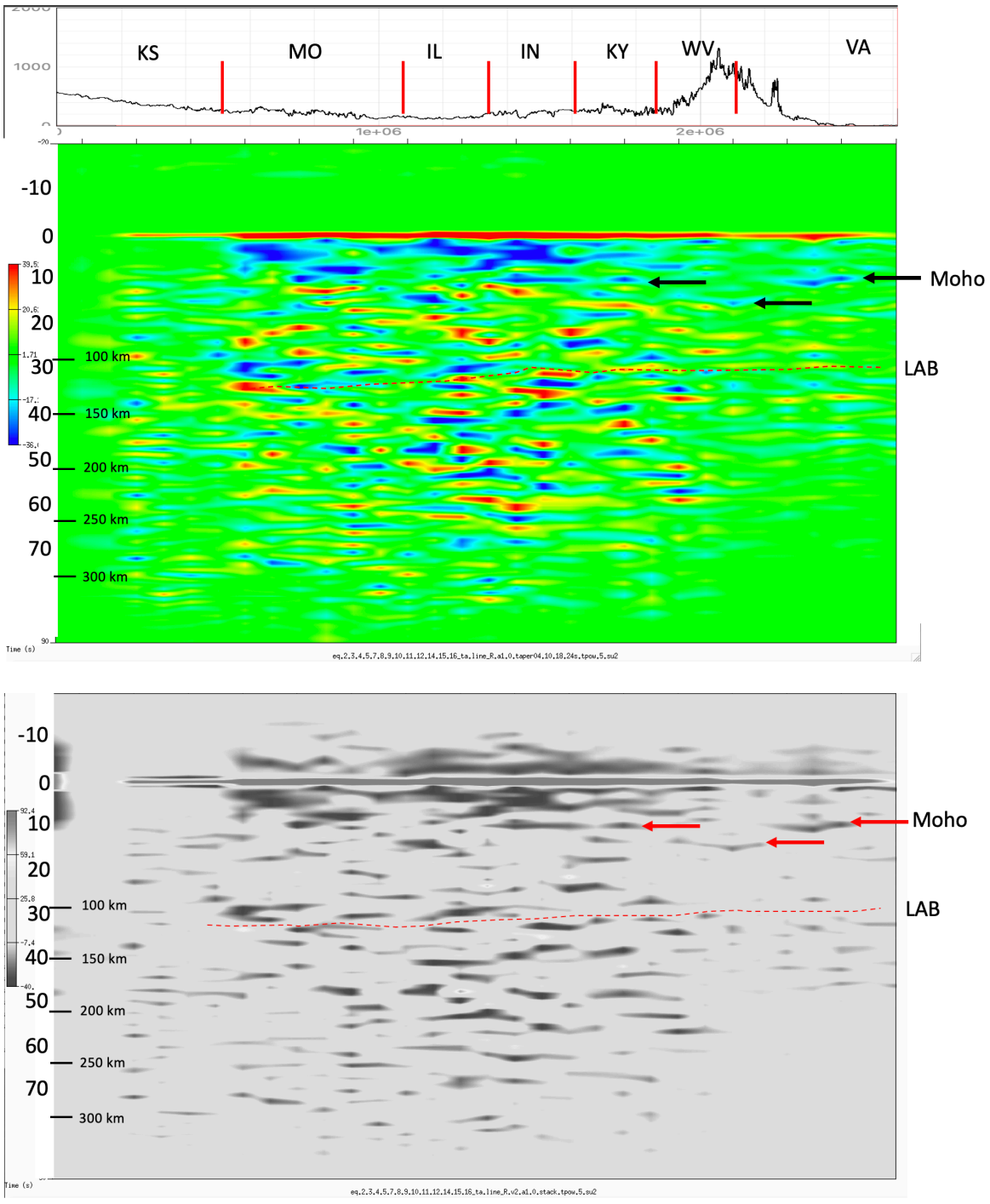

Figure 19- Stacked profile from line R α1 in color and gray scale. This stack shows the crust thickening beneath the Appalachians then thinning west before thickening again. The LAB is marked by the increase in reflectivity.

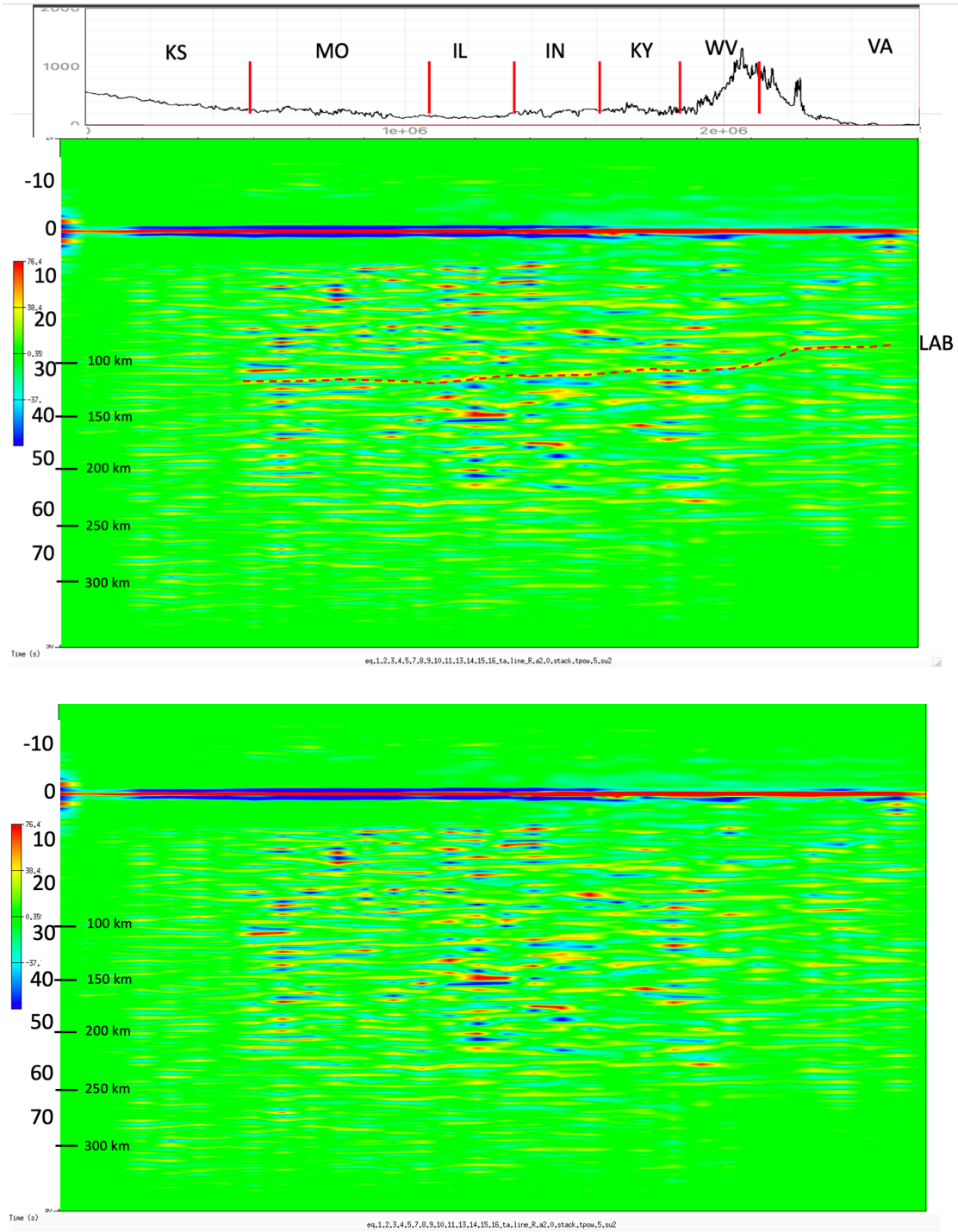

Figure 20- Stacked profile from line R α2. The LAB dips from 100 km to 120 km.

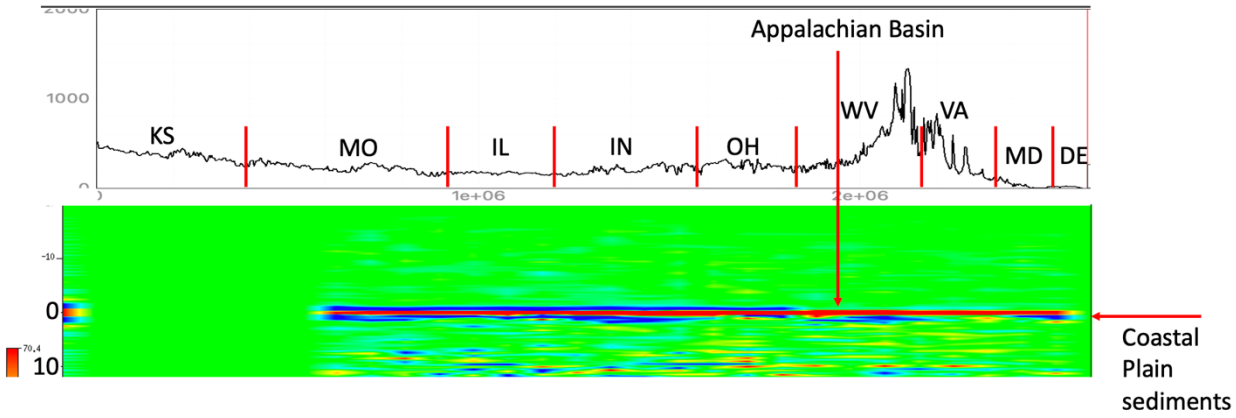

Figure 21- Stacked profile from line Q α3 (cropped to emphasize shallow structure). The base of the Coastal Plain is near 3 km and the base of the Appalachian Basin is at roughly 5 km.

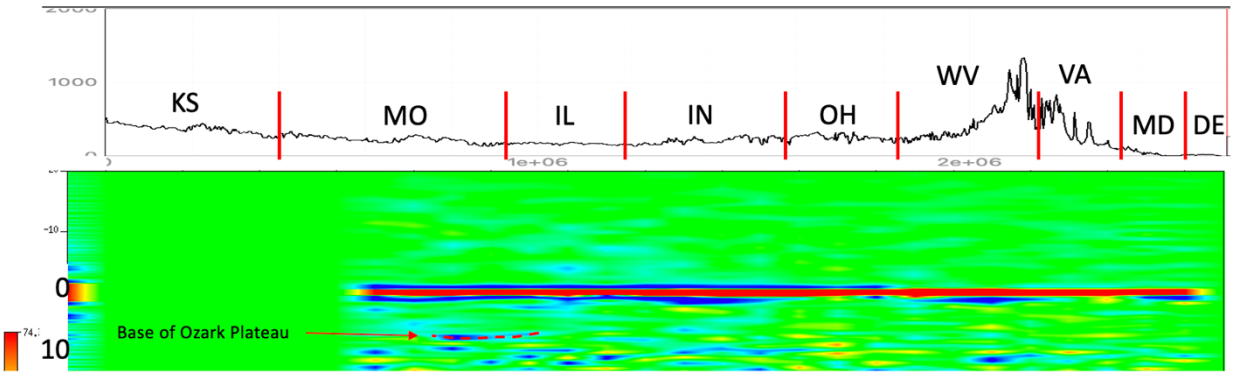

Figure 22- Stacked profile from line Q α2 (cropped to emphasize shallow structure). At 22 km, the base of volcanics associated with the Ozark Plateau appears as a bright blue amplitude.

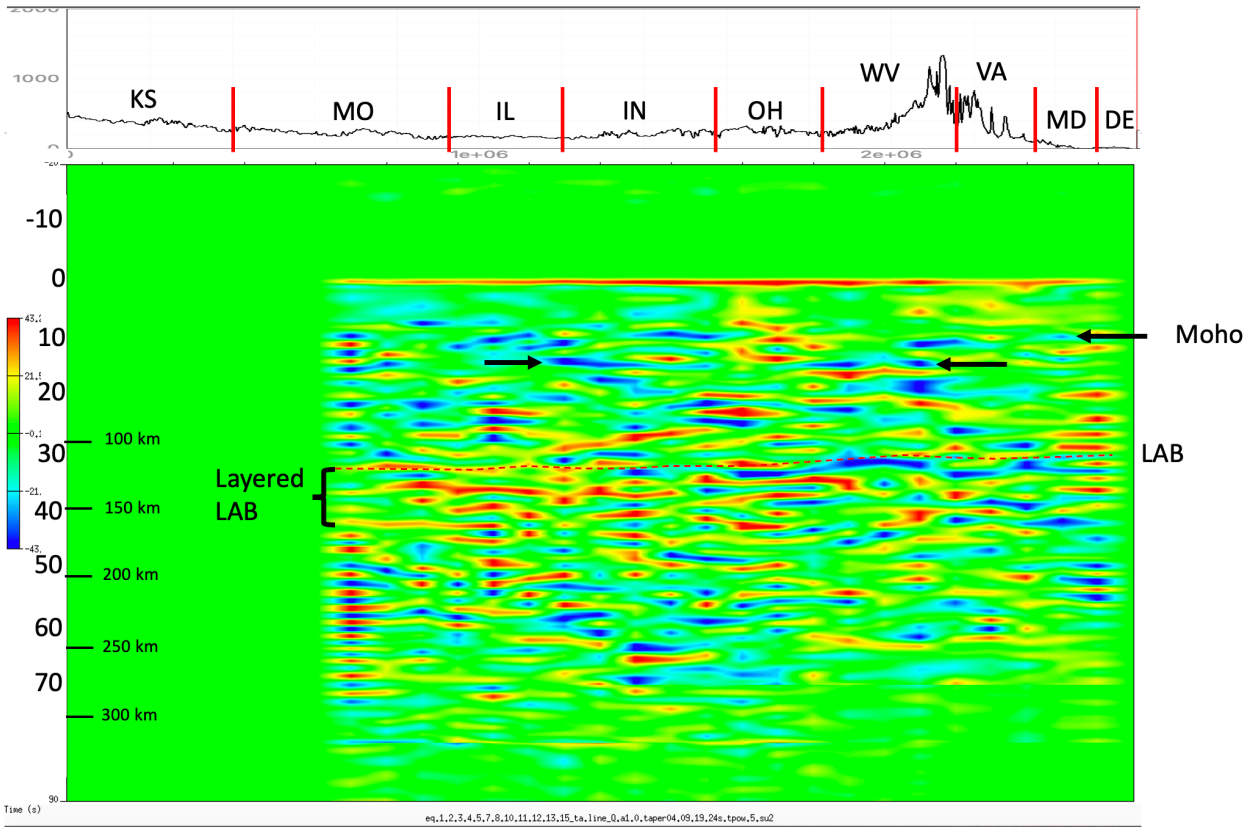

Figure 23- Stacked profile from line Q α1. The Moho deepens from 33 km beneath the Coastal Plain to between 50-55 km from the Appalachian Plateau westward. At the lower frequency value, the LAB is marked by the transition to increased reflectivity and in the west, the zone of positive amplitude indicating a layered boundary.

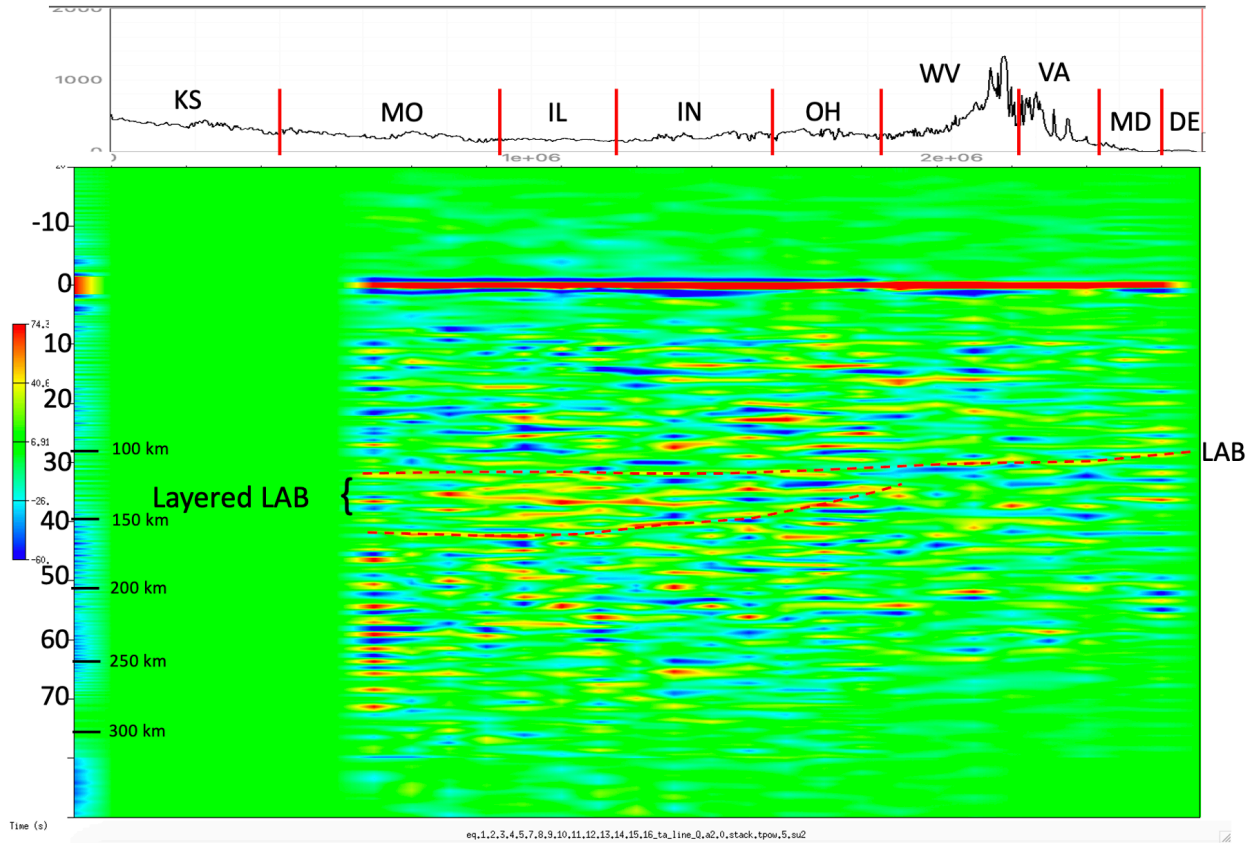

Figure 24- Stacked profile from line Q α2. This image provides a clearer representation of the LAB and its changes in character from east to west. The sharp boundary to the east becomes more gradational to the west, marked by the zone of positive amplitude reflections. Beneath the boundary, reflectivity increases.

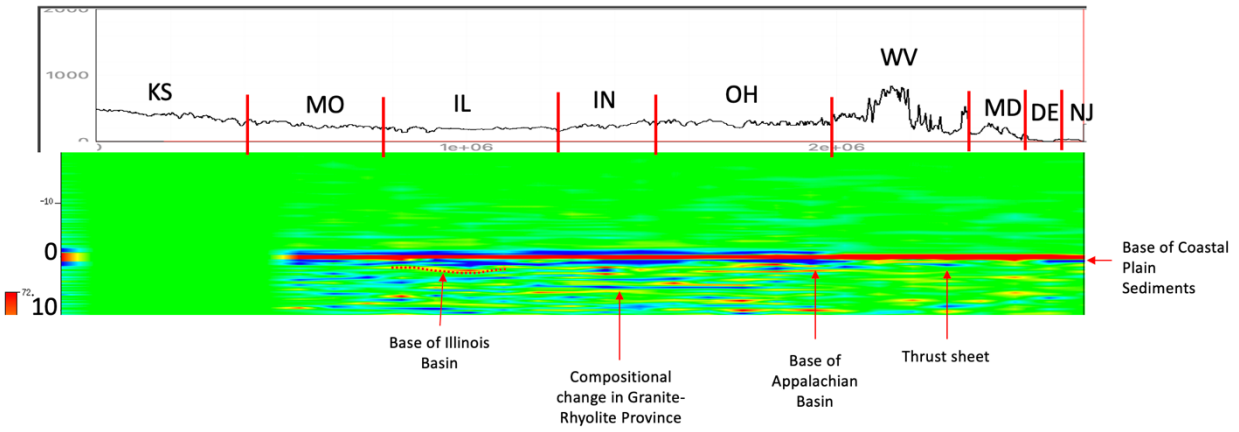

Figure 25- Stacked profile from line P α3 (cropped to emphasize shallow structure). The base of Coastal Plain sediments is at 2 km and begins to narrow east to west. Beneath the eastern panhandle of West Virginia, an east dipping reflection is consistent with a possible thrust sheet. The base of the Illinois Basin is marked by a positive amplitude reflection at 8 km. The reflection at 6 s (19 km) within the Granite-Rhyolite Precambrian province may mark a transition from more felsic upper crust to more mafic below.

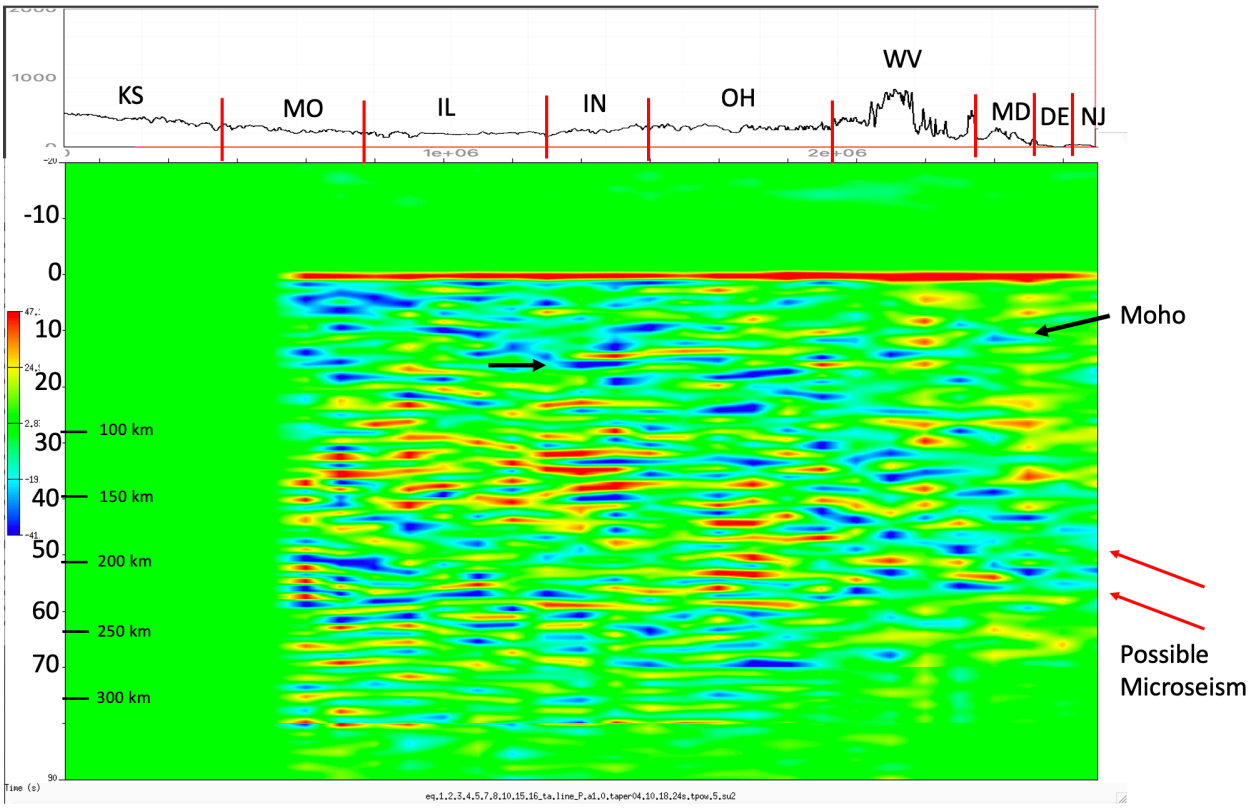

Figure 26- Stacked profile from line P α1. The Moho begins at 30 km beneath the Coastal Plain, dips sharply beneath the Appalachian Mountains to roughly 50 km, before gradually flattening at 55 km moving westward along the array. Arrows mark signals with an eastward apparent dip that likely represent interference associated with microseisms generated by storm activity in the Pacific.

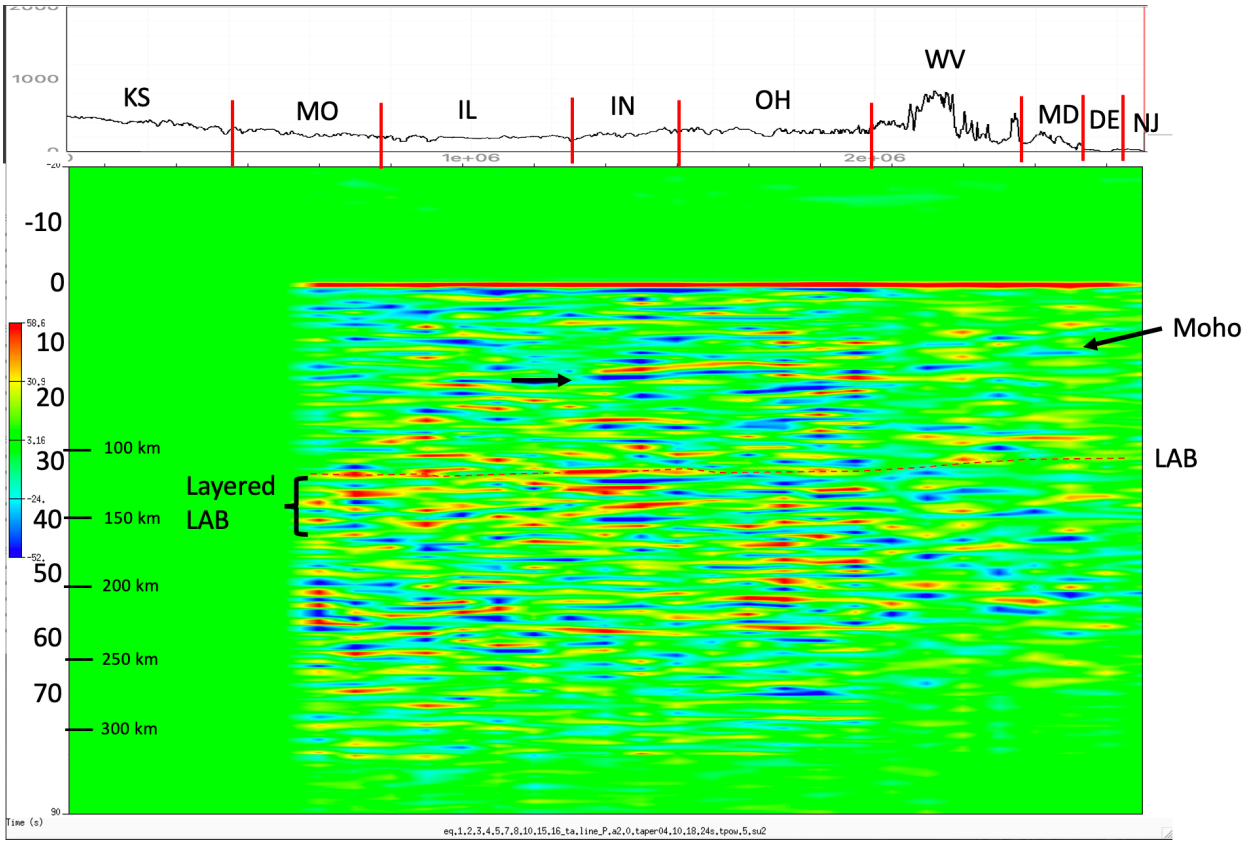

Figure 27- Stacked profile from line P α2. In addition to discontinuous signals interpreted as the Moho, the LAB is more clearly defined at a higher frequency. Increased reflectivity begins at roughly 110 km beneath the eastern portion of the section, then continues below the zone of positive amplitudes to the west that mark the layered transition from lithosphere to asthenosphere. The base of the LAB in this part of the array bottoms out at roughly 155 km.

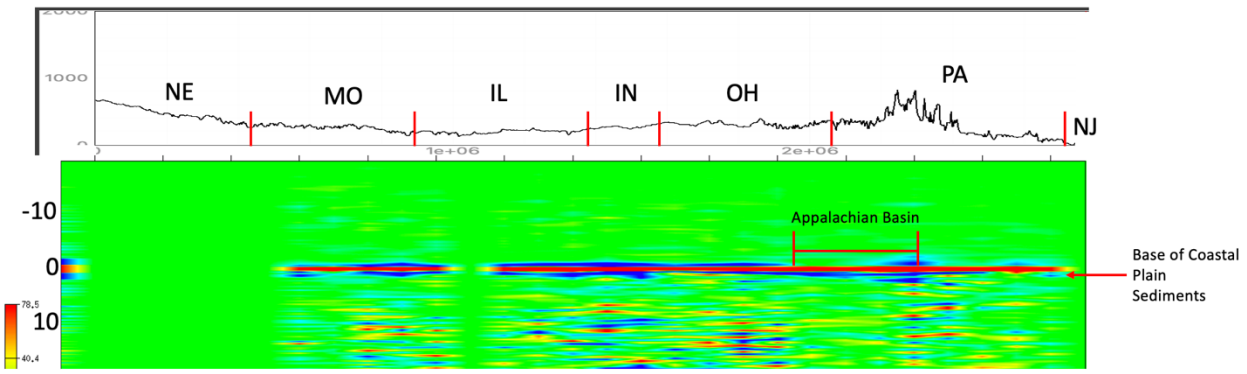

Figure 28- Stacked profile from line O α3. To the east, the small reflection at 2 km indicates a thinning coastal plain moving northward in the study area. Beneath western Pennsylvania and eastern Ohio, a reflection at 5-6 km is consistent with the base of the Appalachian Basin.

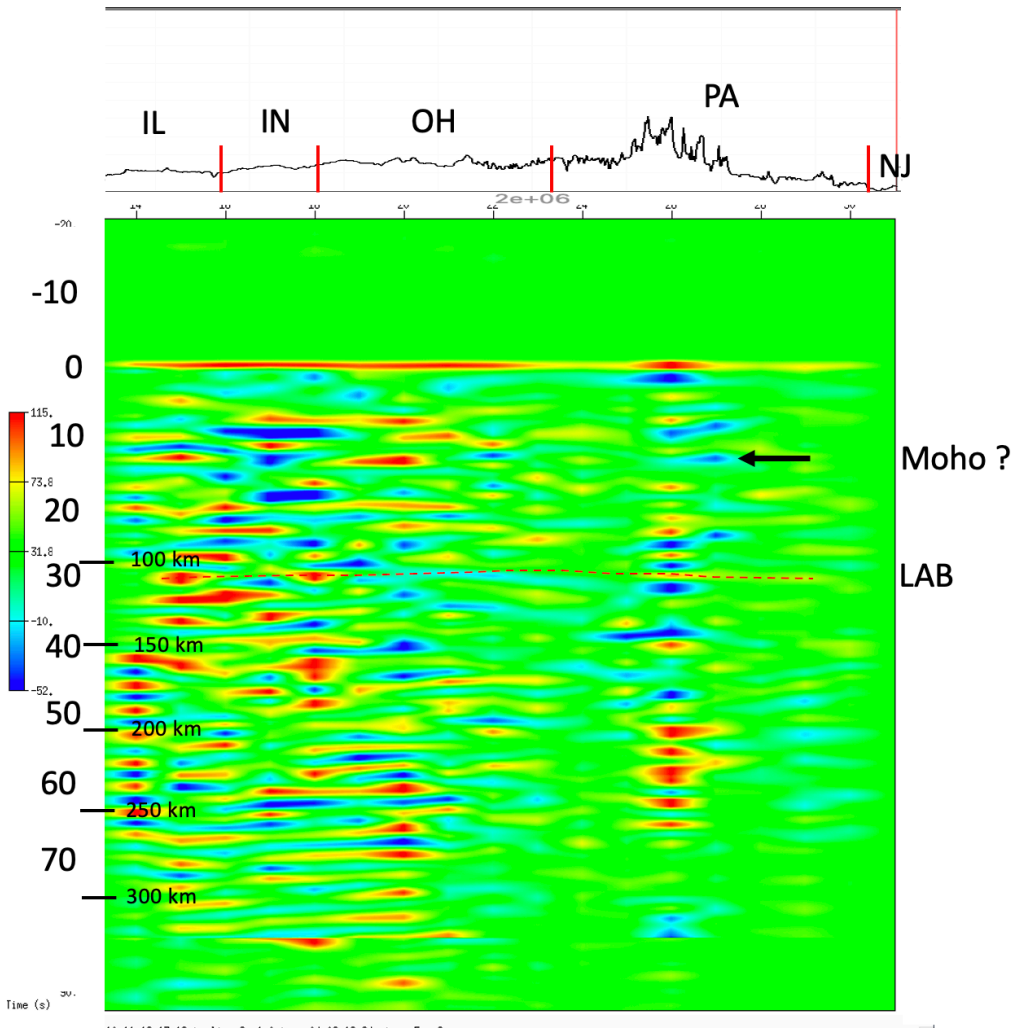

Figure 29- Stacked profile from line O α1 (Note: western part of profile not shown due to poor signal).

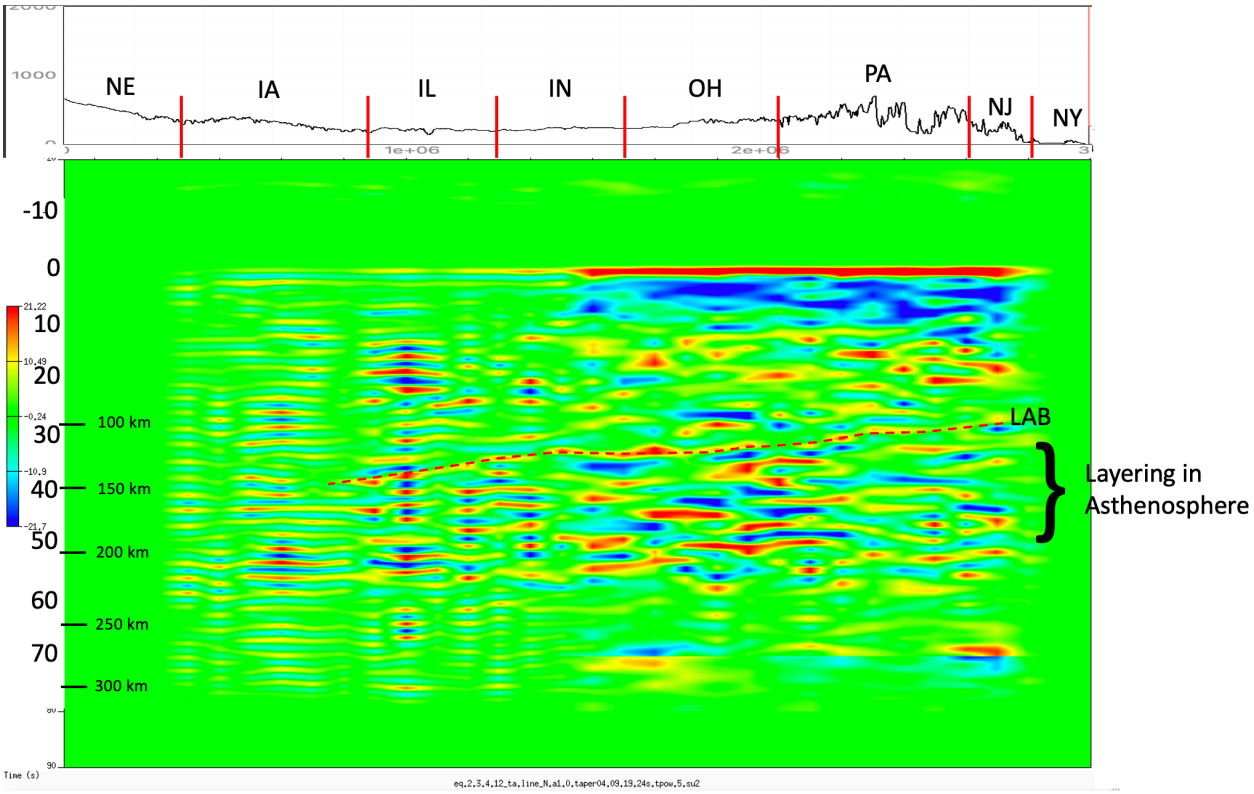

Figure 30- Stacked profile of line N α1. The LAB is marked by the change in reflectivity which we interpret to be layering within the asthenosphere.

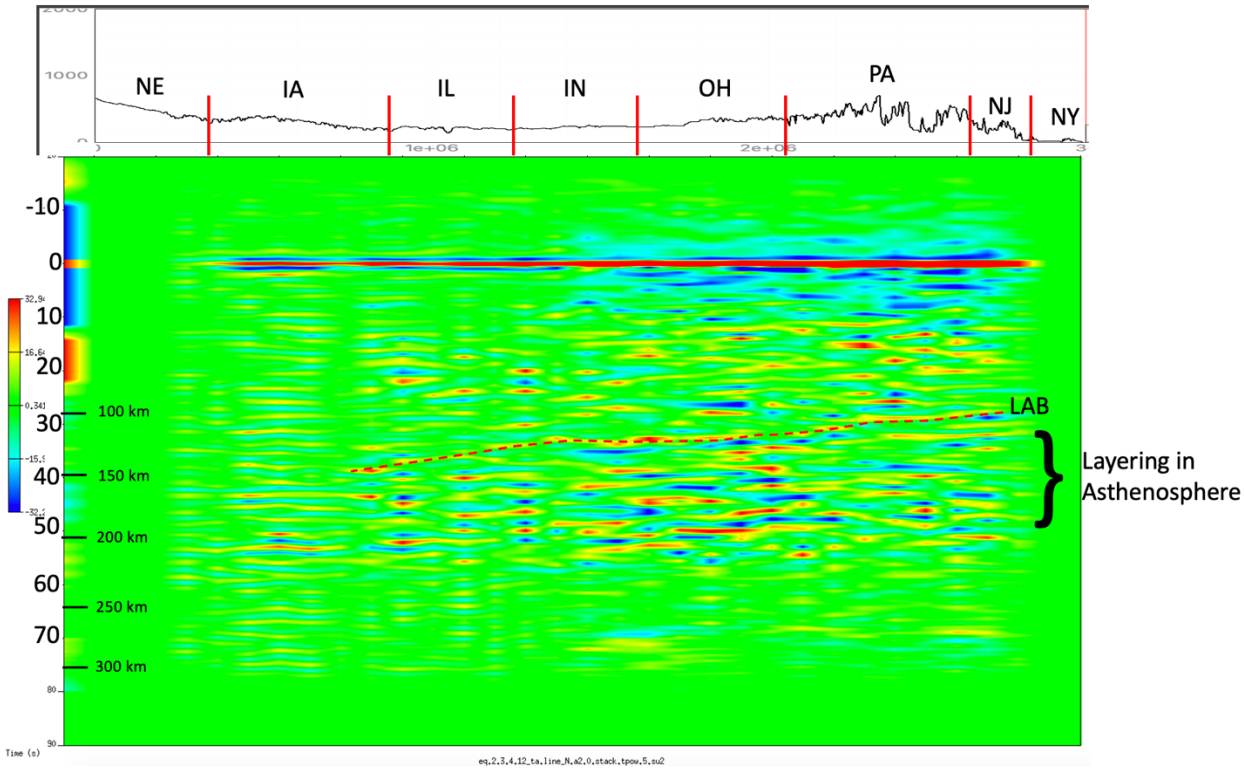

Figure 31- Stacked profile from line N α2. The blue reflections concentrated in the eastern portion of the profile between 0-2 s may be imaging thrust sheets beneath the Pennsylvania Valley and Ridge province. The interpreted LAB is marked by a clear increase in reflectivity from 100 km in the east to 150 km on the western edge of the profile.

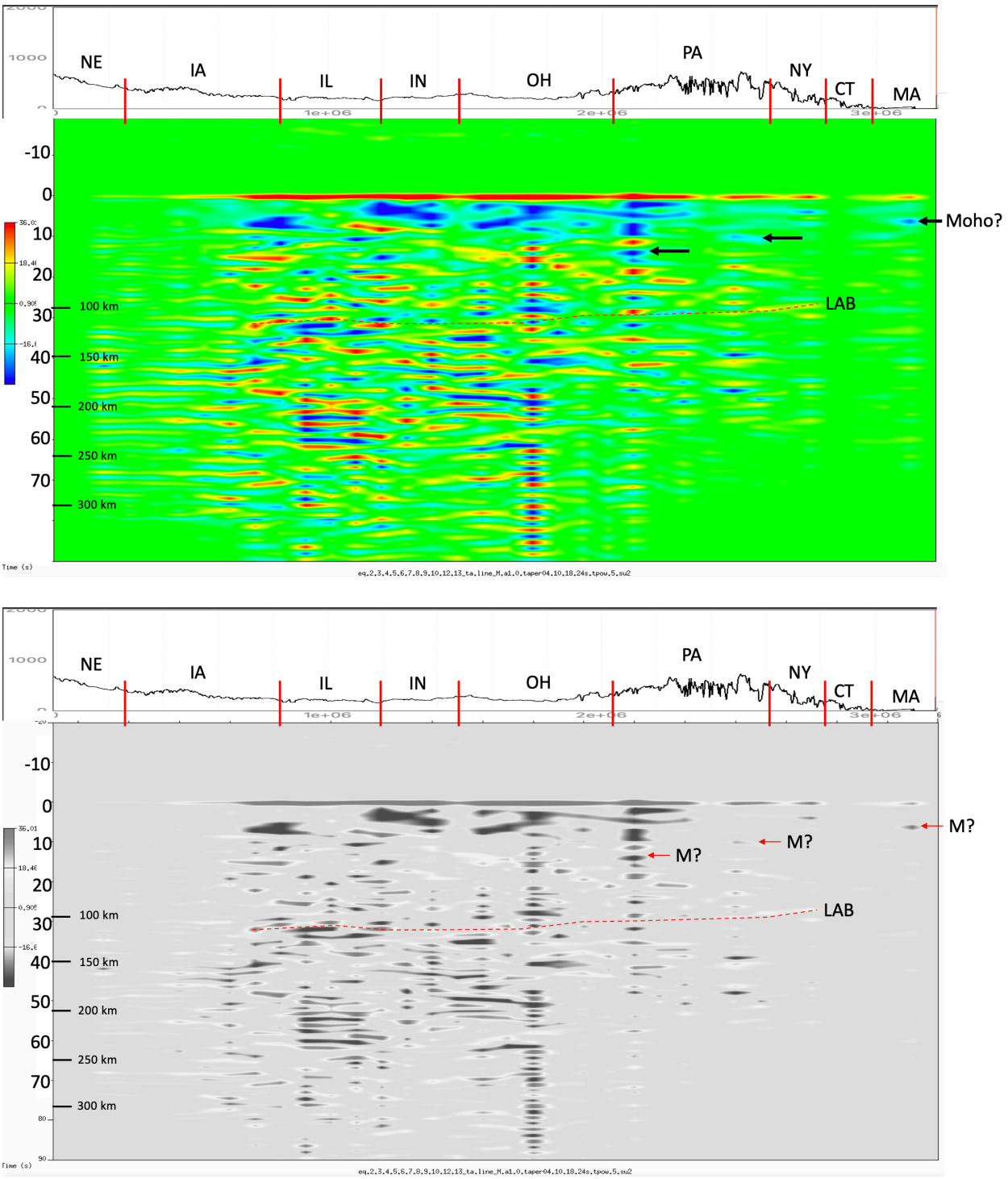

Figure 32- Stacked section from line M α1 in color and gray scale. The LAB is marked by the increase in reflectivity that occurs from 100 km in the east to 110 km to the west.

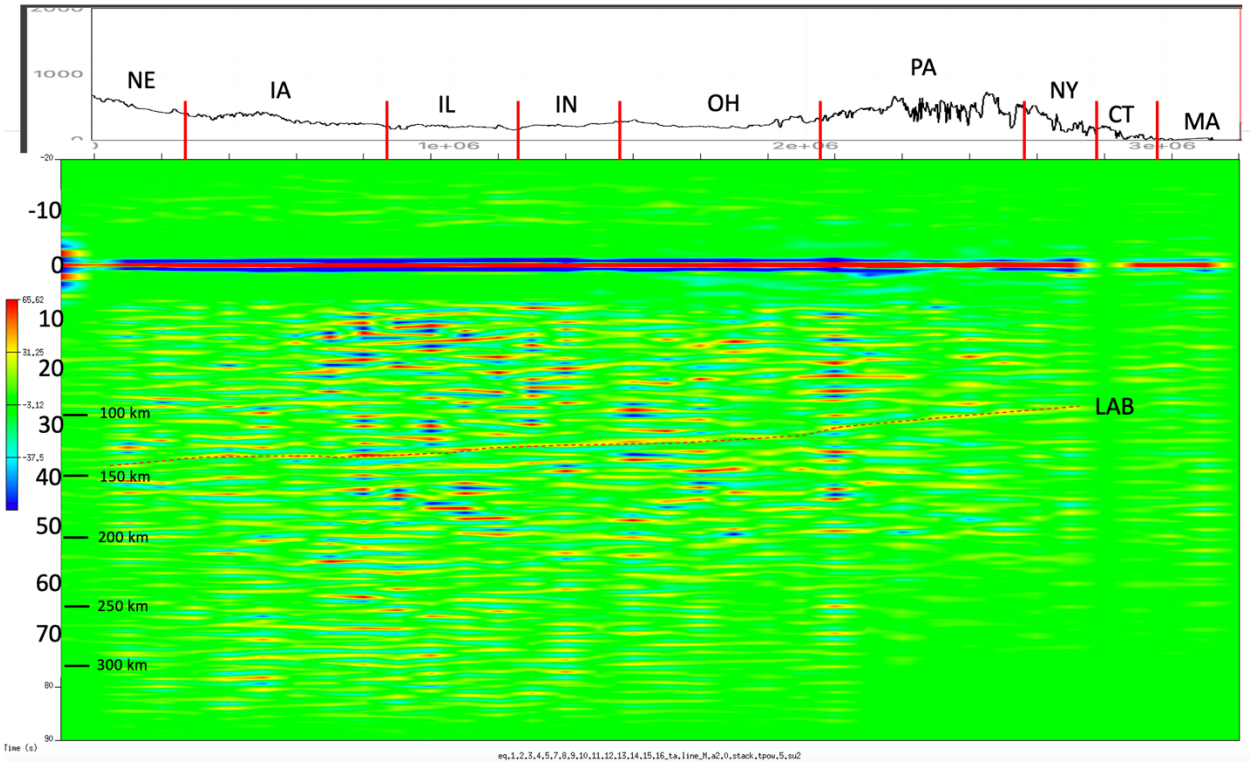

Figure 33- Stacked profile from line M α2. The LAB here is marked by a continuous positive amplitude reflection that crosses the profile dipping westward from 100 km to 145 km.

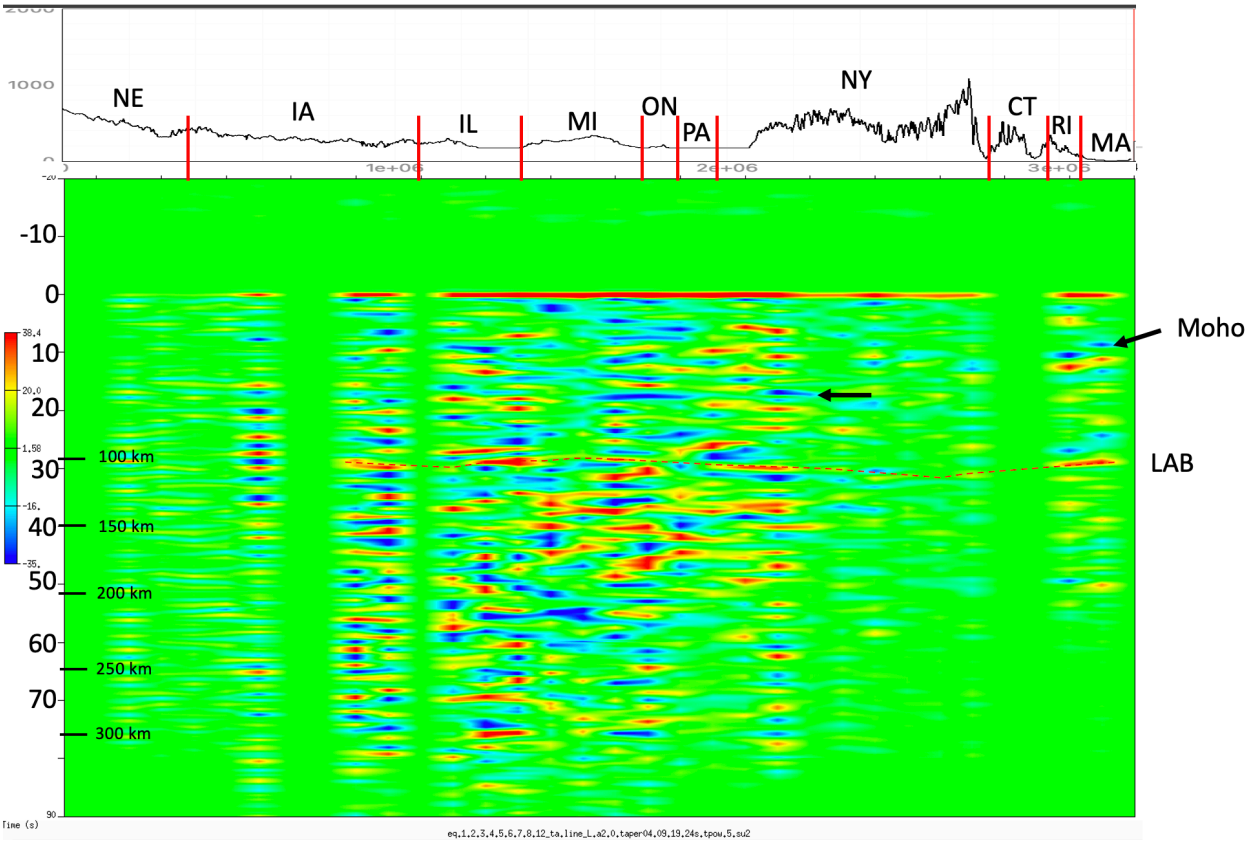

Figure 34- Stacked profile from line L α2. The Moho dips from roughly 25 km beneath Cape Cod in far eastern Massachusetts to about 60 km west of the Appalachian Plateau. The interpreted LAB is between 100 km to 110 km.

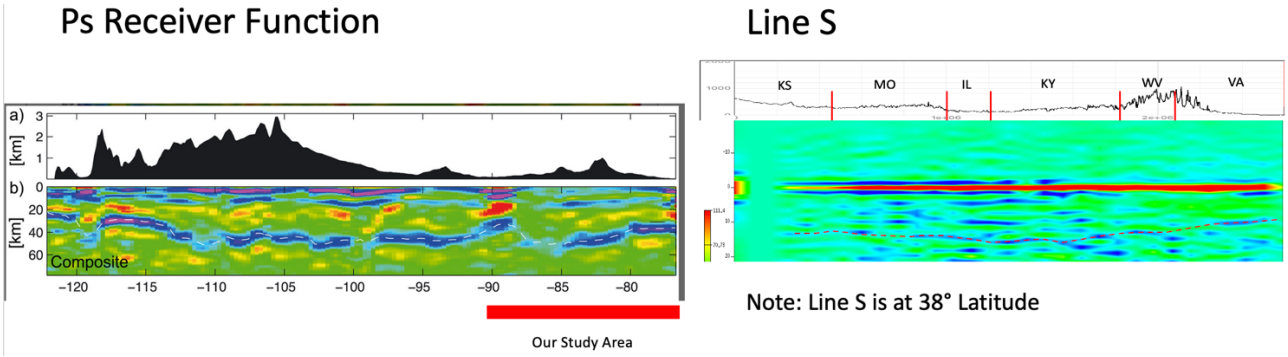

Figure 35- Comparison of Ps receiver function results from Schmandt et al. 2015 with our results. Their profile is 3° south of our study area, but the Moho shows a similar geometry where the crust thickens beneath the Appalachian Mountains.

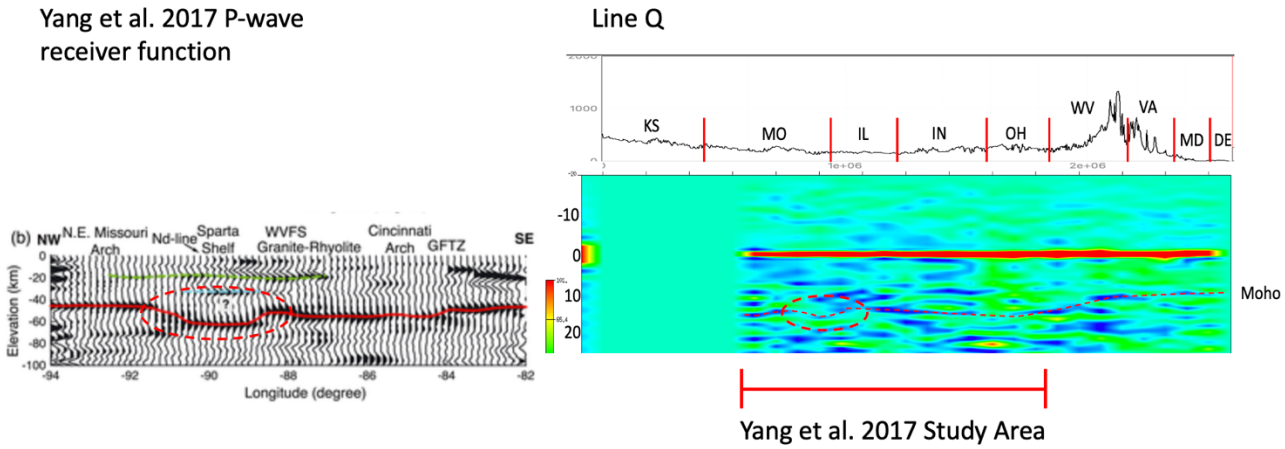

Figure 36- Comparison of P-wave receiver function analysis by Yang et al. 2017. Both profiles show a localized thickening of the crust beneath the western edge of the Illinois Basin.

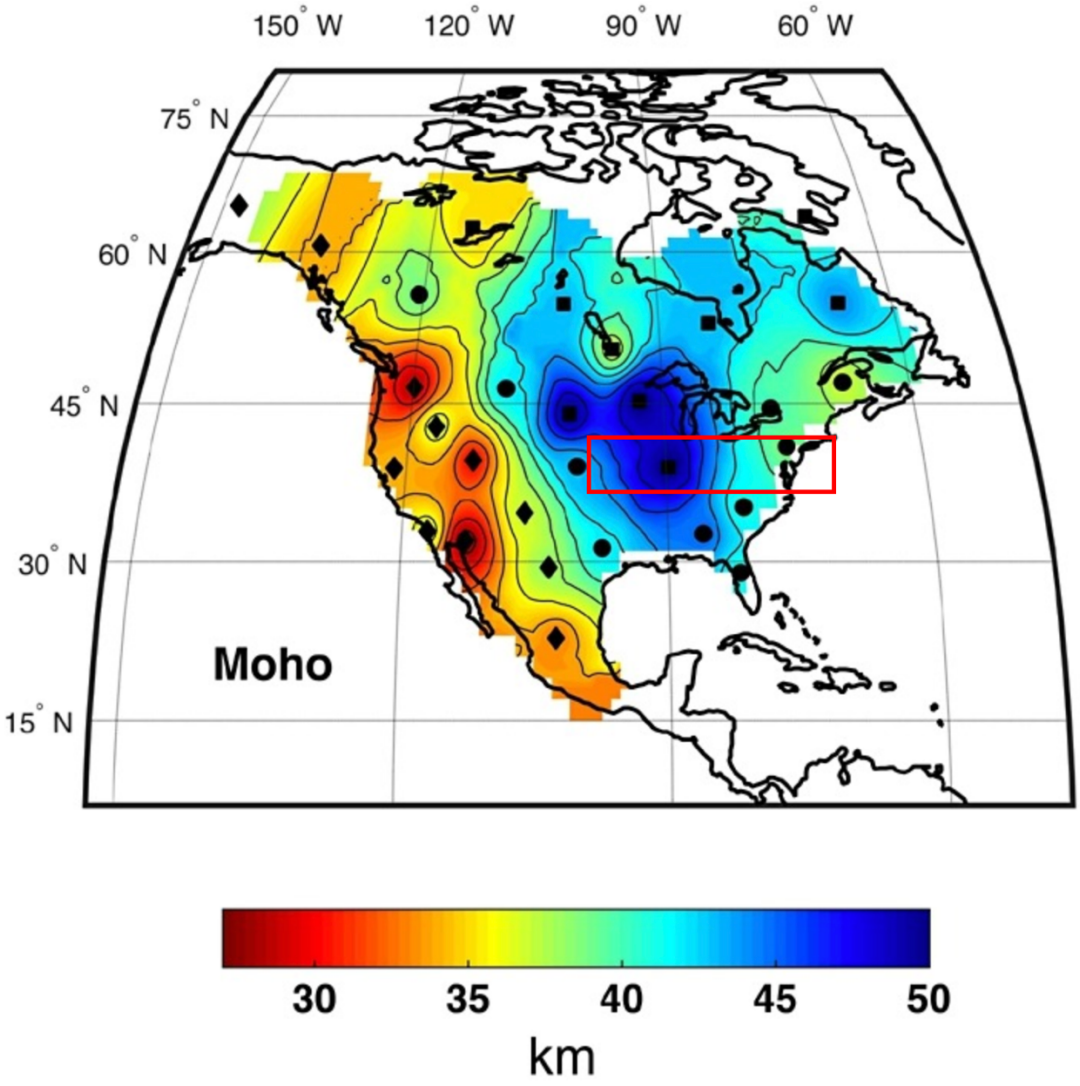

Figure 37- Map of Moho depth from Calo et al. 2016. Our study area is outlined by the red block.

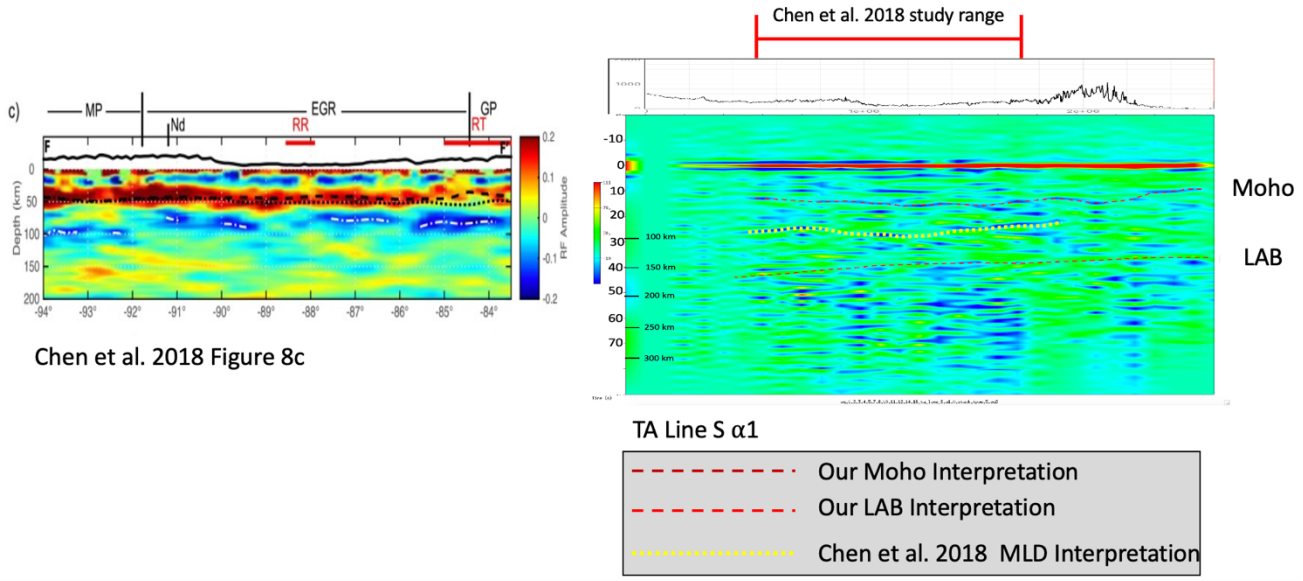

Figure 38- Comparison of our results from line S with Sp receiver function amplitude results from Chen et al. 2018. The higher resolution of our results shows the LAB clearly where the Sp receiver function is unable to resolve the boundary.

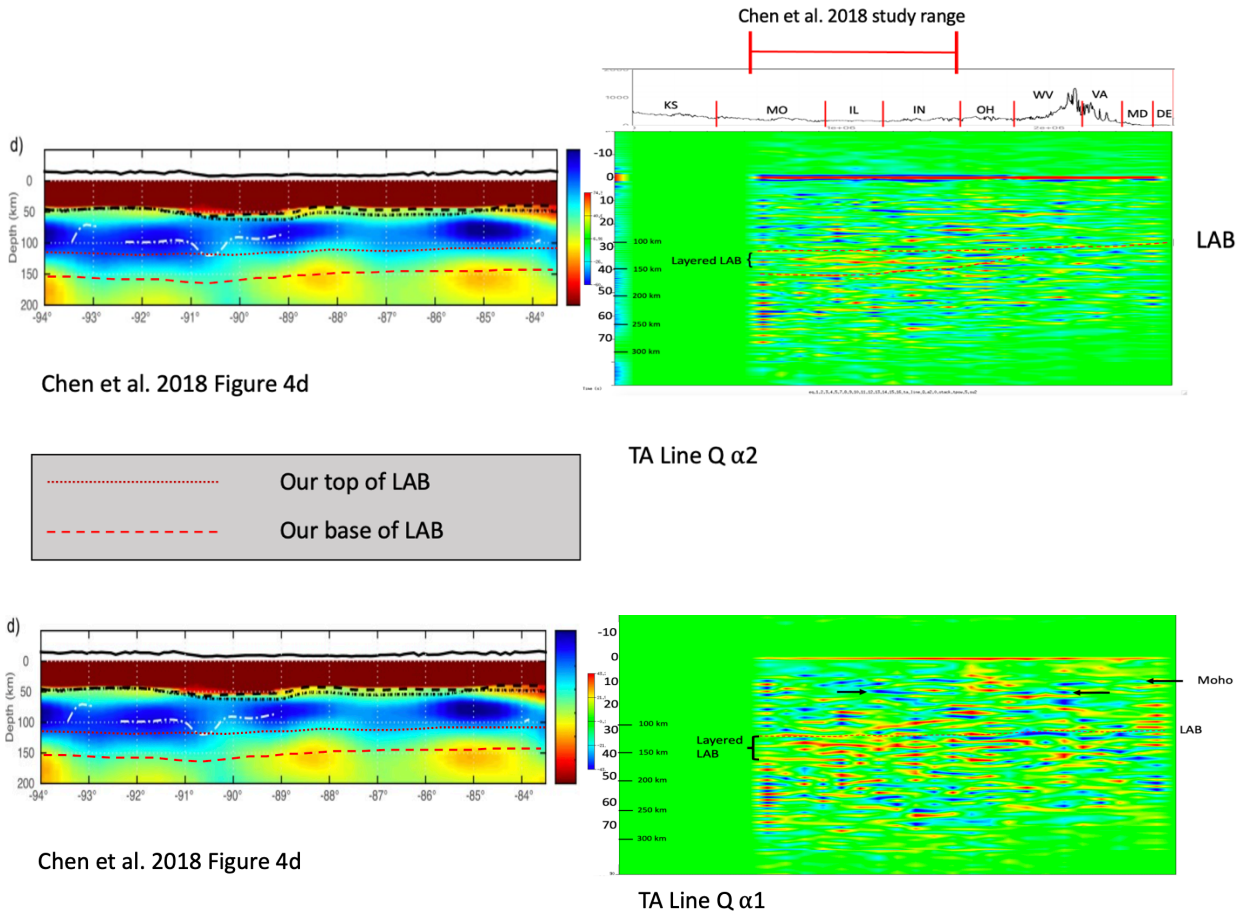

Figure 39- Comparison of results from line Q with shear wave velocities derived by tomography (Chen et al. 2018). Overall, our interpreted LAB which is defined as the top of a zone of increased reflectivity, correlates with the maximum negative velocity gradient in the tomography model.

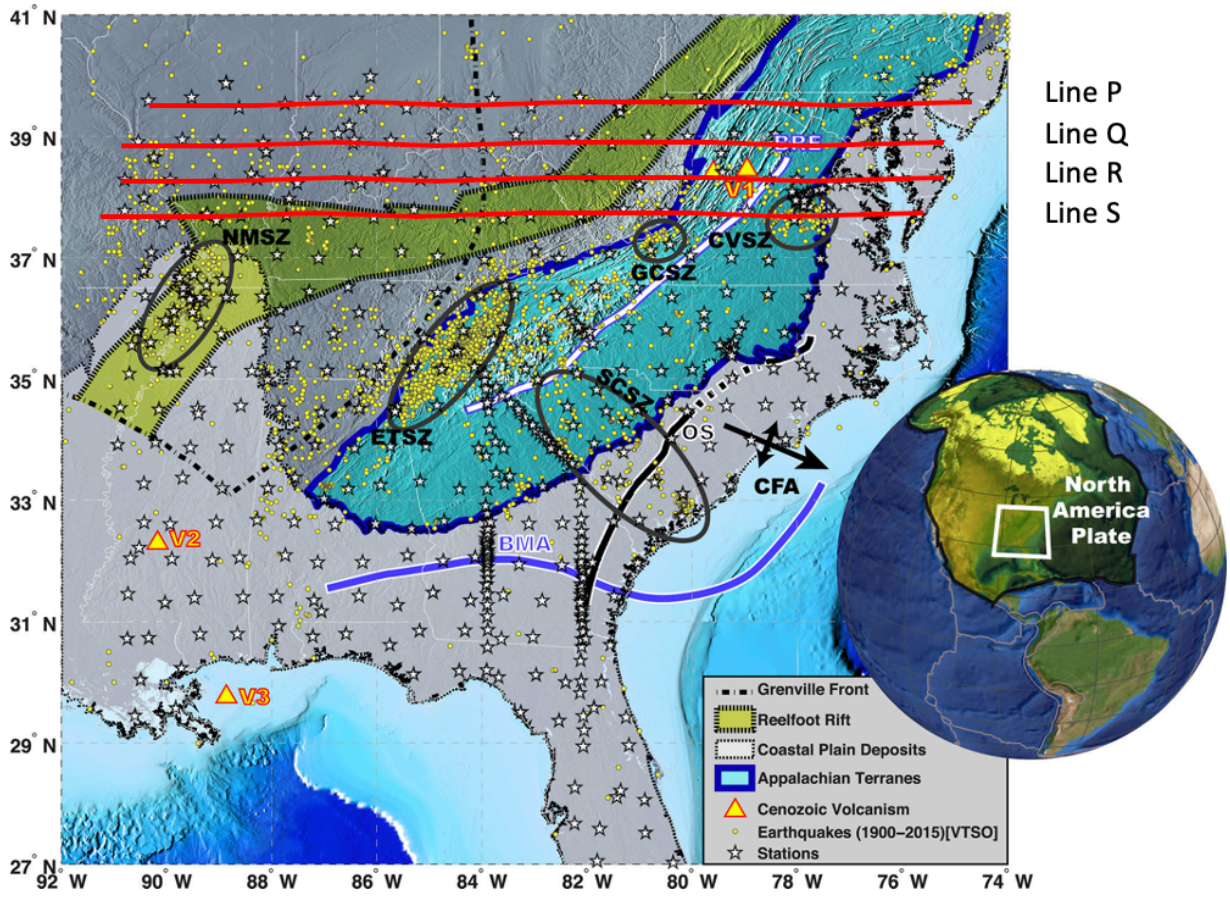

Figure 40- Figure adapted from Biryol et al. 2016 showing the lines from our study that traverse geologic features of interest including Eocene volcanics in western Virginia and to zones of increased seismicity: the Central Virginia Seismic Zone (CVSZ) and the Giles County Seismic Zone (GCSZ).